Theory of the longitudinal and Hall conductivities of the cuprate superconductors

Branko P. Stojković and David Pines
Department of Physics and Materials Research Laboratory, 1110 West Green Street, University of Illinois, Urbana, Illinois 61801
(Received 16 September 1996)

We establish the applicability to transport phenomena in the cuprate superconductors of a nearly antiferromagnetic Fermi liquid (NAFL) description of the magnetic interaction between planar quasiparticles by using it to obtain the doping- and temperature-dependent resistivity and Hall conductivity seen experimentally in the normal state. Following a perturbative calculation of the anisotropic (as one goes around the Fermi surface) quasiparticle lifetimes which are the hallmark of a NAFL, we obtain simple approximate expressions for the longitudinal, σ_{xx}, and Hall, σ_{xy}, conductivities which reflect the magnetic crossovers seen experimentally as one varies the doping level and temperature. We present a simple phenomenological model for the variation in the mean free path around the Fermi surface and use this to extract from experiments on σ_{xx} and σ_{xy} quasiparticle lifetimes in the hot (strongly coupled quasiparticle) and cold (weakly coupled quasiparticle) regions of the Fermi surface which are consistent with the perturbation theory estimates. We improve upon the latter by carrying out direct numerical (nonvariational) solutions of the Boltzmann equation for representative members of the $YBa_2Cu_3O_{6+x}$ and $La_{2-x}Sr_xCuO_4$ systems, with results for transport properties in quantitative agreement with experiment. Using the same numerical approach we study the influence of CuO chains on the *a*-*b* plane anisotropy and find results in agreement with experimental findings in $YBa_2Cu_4O_8$. [S0163-1829(97)04413-5]

I. INTRODUCTION

The peculiar normal state properties of high-temperature superconductors (HTS's) have been extensively studied over the past decade in the expectation that their understanding will likely reveal the mechanism of superconductivity. Yet no consensus has emerged as to their physical origin. Indeed, it is striking that so much work has been done on understanding a variety of complicated experimental situations, while rather basic measurements, such as the dc transport, are not well understood. So far it has been clearly established[1] and well documented in the literature[2–4] that practically all normal state properties in these materials are anomalous with respect to the behavior of standard Landau Fermi liquids (FL's). This, in turn, poses the question of whether Landau FL theory is applicable to HTS's.[5] A variety of proposals based on non-Fermi-liquid[6–8] (NFL) or marginal FL (Ref. 9) theories have emerged which have had considerable success in explaining a number of specific experimental results. However, at present no single theory has been able to account for *all* the anomalies found in the normal state properties of the cuprates.

In this paper we focus on the planar resistivity and the Hall effect, which have drawn particular attention in the HTS community, due to their arguably ''contradictory'' behavior:[10] The temperature dependences of the Hall angle θ_H and the longitudinal resistivity ρ_{xx} are so vastly different that the Hall coefficient R_H in practically all cuprates is a strong function of temperature, especially near optimal doping. This phenomenon by itself is rarely observed in ordinary FL's.[11] It is also found that all HTS's near optimal doping have ρ_{xx} proportional to the temperature T in a wide region of interest. Hence it appears that transport properties in the presence of a magnetic field as well as in its absence require two separate scattering mechanisms and, presumably, two separate relaxation rates. In fact this is the only common scheme among the competing theories for the explanation of the anomalous transport in HTS materials.

We begin with a brief review of the theoretical proposals. Anderson, who drew attention to the problem of explaining the unusual magnetotransport in the normal state,[10] has proposed a scenario based on a NFL ground state. In his scenario the two rates observed in experiment are attributed to scattering of two distinct many-body excitations, *spinons* and *holons*. The existence of these excitations is well established in one-dimensional (1D) Luttinger liquids and Anderson has put forth a nontrivial generalization of this concept to the quasi-two-dimensional system found in cuprate superconductors. Strictly speaking one can talk about a NFL in any system at or near half-filling, which has an interaction sufficiently strong to produce the Néel instability, but the validity of this approach at large doping levels is somewhat questionable. In the Anderson scenario both spinons and holons contribute to the resistivity, but it is often tacitly assumed that the scattering of holons dominates, while only spinons, which effectively commute with the magnetic field B, appear in the temperature variation of the Hall angle. Although commonly used to analyze experiments, this proposal has yet to be verified by an explicit calculation of the transport coefficients.[12]

Coleman *et al.*[13] have developed a phenomenological transport theory based on the assumption that the dominant scattering in cuprates is mediated by an interaction which distinguishes quasiparticle wave functions with respect to their charge conjugation symmetry. Such interactions are absent in ordinary FL's and hence this can be regarded as a NFL model, although in this case there is no spin-charge separation and hence the model is more correctly categorized as an *unusual* FL. In this model quasiparticles with different symmetry have vastly different scattering rates, which in turn

have different temperature dependences, ultimately leading to the correct behavior of all transport coefficients. Although the origin of the unusual interaction has not been identified, this is the only model to date which appears to be consistent with recent experimental results on optical reflectivity.[14]

The anomalous Hall effect can also be understood in terms of the bipolaron theory, developed by Alexandrov, Bratkovsky, and Mott.[15] Anomalous behavior in their model arises from Anderson localization of bipolarons: At low temperatures bipolarons in a random potential lose their mobility, producing an enhanced value of R_H. At sufficiently high temperature, larger than the random potential binding energy, the mobility is recovered, and R_H saturates, as seen in experiment. The bipolaron model is also consistent with a number of photoemission experiments.

A variety of FL-based models have also been utilized to explain the anomalous transport in cuprates. Clearly, in order to account for experiments, one must introduce the *two* scattering rates without violating the FL ground state. This is done either by introducing a certain anisotropy of scattering or by assuming a different mechanism of scattering in the presence of a magnetic field. Initially, the anomalous Hall effect was attributed to the well-known skew scattering present in many materials with strong spin-orbit coupling;[16] the anomalous temperature variation of ρ_{xy} arises from anisotropic scattering of conduction electrons by local magnetic moments. This approach naturally produces the observed temperature dependence of ρ_{xy}, provided the resistivity is assumed linear in T. However, one runs into problems for systems with doping levels for which the resistivity is not proportional to temperature. Moreover, skew scattering should saturate with increasing magnetic field, due to the complete polarization of localized moments. Such saturation has not been observed, although some discrepancy from the linear-in-B Hall resistivity does occur in extremely high pulsed fields.[17]

Levin and Quader[18] focused on a very important subgroup, the bilayer cuprates. In their approach the anomalous behavior of the Hall effect is due to the multiband structure of bilayer cuprates. Their main assumption is that one of the bands is very close to the Fermi level and responsible for the anomalous resistivity, while the other is responsible for the Hall angle. The former is thermally activated at higher temperatures in underdoped materials so that the model can explain qualitatively the behavior of resistivity in the underdoped bilayers. Although their approach appears reasonable, the striking similarity between the experimental results on single-layer and bilayer materials, which we discuss in Sec. IV, indicates that this approach may have to be revised before it possesses general applicability.

Another class of models is based on anisotropic scattering, which can arise from either anomalous band structure in the cuprates or spin-fluctuation scattering. Newns *et al.*[19] have proposed a model based on an anomalously large density of states near the Fermi surface (FS) for quasiparticles in the vicinity of the so-called Van Hove singularities: Angle-resolved photoemission spectroscopy (ARPES) experiments in a number of samples show extended flat band features near $k=(\pi,0)$ and symmetry-related points in the Brillouin zone, which give rise to highly anomalous quasiparticle scattering. The two scattering rates necessary to explain the measured transport properties are those for quasiparticles near and far away from these singularities. Although the model can produce a temperature-dependent Hall coefficient $R_H \equiv \rho_{xy}$, it is unclear whether it can simultaneously account for the anomalous behavior of the resistivity.

We next consider models based on spin-fluctuation scattering. One of the first contributions has been provided by Carrington and collaborators[20] who used a phenomenological model of the spin fluctuations and a realistic FS and calculated a number of transport coefficients in cuprates. They assumed that large parts of the FS have an anomalous, linear-in-T scattering rate, while smaller parts have a Fermi-liquid, quadratic-in-T scattering rate. Although the anomalous quasiparticle scattering rate, assumed to be due to spin fluctuations, has been taken as an input to the theory, they obtained a remarkable agreement not only with the Hall effect, but with the thermoelectric power as well. This work motivated a number of authors to explore more particular choices of spin-fluctuation spectra and their relationship with transport.[21–23]

Trugman[24] calculated the band structure renormalization in the presence of strong antiferromagnetic (AF) fluctuations within the context of the t-t'-J model and obtained a single-particle band structure which has the form of a precursor to a spin-density-wave (SDW) state. In this case one finds flat regions in the band, somewhat similar to those mentioned above, which are characterized by an energy scale which is much smaller than the fermionic bandwidth. In essence the size of the Fermi energy is effectively reduced to an energy $\Omega \ll t$, and hence, just as in ordinary FL's, the resistivity deviates from its usual T^2 dependence, while the Hall coefficient is temperature dependent. However, we note that this anomalous temperature dependence of the Hall effect is primarily due to the strong anisotropy of scattering rates and densities of states in different regions of the Brillouin zone. Similar models were also provided by Kim *et al.*[25] and by Dagotto *et al.*[26]

Lercher and Wheatley[22] also studied a spin-fluctuation model of magnetotransport in the cuprates. They concluded that the behavior of several quantities of interest is significantly altered depending on whether or not one incorporates umklapp processes. At high temperatures they find a highly T-dependent Hall coefficient, with a resistivity approximately linear in T. As in the above cases, their calculation is based on the anisotropy of scattering rates in different regions of the Brillouin zone, although here the anisotropy originates in the specific structure of the effective interaction.

The nearly antiferromagnetic Fermi liquid (NAFL) model for transport in the cuprates resembles the model studied by Lercher and Wheatley, as well as the earlier Hubbard model calculations of the resistivity by Bulut, Scalapino, and White,[27] with one important difference: the choice of the effective interaction. Although in both cases the effective quasiparticle interaction $V_{\rm eff}$, assumed to be of magnetic origin, is a strong function of momentum transfer and is highly peaked near the antiferromagnetic wave vector $\mathbf{Q}$, Lercher and Wheatley calculate $V_{\rm eff}$ using a random phase approximation (RPA) formalism with a local restoring force, while in the NAFL model one takes the momentum and frequency dependence of the interaction to be that of the spin-spin response function which provides a quantitative account of the

NMR experiments,[28] as discussed in the next section. While a RPA formalism can provide insight into the physical origin of the spin fluctuations, it neglects changes in the effective interaction brought about by the spin-fermion vertex corrections, which lead to a sequence of crossovers in the low-frequency magnetic behavior in the normal state.[29] Thus it is not capable of accounting for the rich morphology of the magnetic properties seen in NMR experiments,[2] a morphology which we shall see is reflected in transport experiments.

Calculations of the resistivity of $YBa_2Cu_3O_7$ using a NAFL model were carried out by Monthoux and Pines,[30] who found, in a strong-coupling (Eliashberg) calculation which incorporated vertex corrections, that a good quantitative account of experiment could be obtained using a spin-fluctuation spectrum taken from NMR experiments and a coupling constant which yielded a superconducting transition at 90 K. This work provided an important bridge between the anomalous normal state properties and the superconducting transition. There remained the important question of whether a NAFL model could also account for the anomalous Hall effect. The present authors addressed this question by using standard Boltzmann transport theory to calculate both the resistivity ρ_{xx} and the Hall conductivity σ_{xy} of $YBa_2Cu_3O_7$.[23] A direct (nonvariational) numerical solution of the Boltzmann equation (BE) showed that the highly anisotropic quasiparticle scattering at different regions of the Fermi surface (brought about by the highly anisotropic magnetic quasiparticle interaction which characterizes a NAFL) could give rise qualitatively, and in some cases quantitatively, to the measured anomalous temperature dependence of the resistivity and Hall coefficient while yielding the quadratic temperature dependence of the Hall angle.[23,31] The present paper extends these calculations in a number of ways. First, we use perturbation theory to calculate, for a broad range of doping and temperature regimes, the anisotropic quasiparticle scattering rates around the Fermi surface; we then use these results to calculate the longitudinal and Hall conductivities. Our perturbation theory approach not only makes explicit the difference in quasiparticle behavior at hot spots (those regions of the FS for which the magnetic interaction is anomalously large) and in cold regions (the remaining parts of the FS), but enables one to examine in detail the changes in quasiparticle lifetimes in both regions brought about by both the crossovers in the spin-fluctuation spectra measured in NMR experiments and the changes in FS shape measured in experiments using angle-resolved photoemission techniques. On taking the relevant averages of quasiparticle lifetimes for the longitudinal and Hall conductivities, we are then able to obtain simple approximate expressions for these quantities as a function of doping and temperature which are in good agreement with experiment.

The substantial anisotropy of quasiparticle mean free paths found in the perturbation theory approach led us to develop a phenomenological model for the variation in mean free path as one goes around the FS and to use this to extract from experiments on σ_{xx} and σ_{xy} the behavior of the quasiparticle lifetimes $\tau_{\rm hot}$ and $\tau_{\rm cold}$ as one varies temperature and doping level for the $YBa_2Cu_3O_{6+x}$ (123), $La_{2-x}Sr_xCuO_4$ (214), and Tl-doped systems. Again, good agreement is found between the perturbation theory estimates and the experimental results.

Guided in part by perturbation theory results and our phenomenological model, we then carry out direct numerical solutions of the BE for representative members of the 123 and 214 systems, and for a highly simplified model of a system, such as $YBa_2Cu_4O_8$ (124), in which the presence of chains brings about considerable planar anisotropy. For all three cases considered, good agreement is found between theory and experiment.

The paper is organized as follows: In the next section we provide the necessary background on the signatures of the NAFL model in NMR experiments and define the relevant crossover temperatures. In Sec. III we analyze the properties of NAFL's using a simple perturbative approach. In Sec. IV we review experimental results found for the 123, 214, and overdoped Tl systems, and call attention to the regularities (or lack thereof) which $\rho_{xx}(T)$ and $\rho_{xy}(T)$ exhibit as a function of doping and temperature. We then present our phenomenological analysis of σ_{xx} and σ_{xy} in terms of a highly anisotropic mean free path and use this analysis to extract from experiment the quasiparticle lifetimes in the hot and cold regimes. In Sec. V, we present numerical calculations for a realistic set of band and spin-fluctuation parameters, and compare our results to experiment. Finally, in Sec. VI we summarize our conclusions.

II. BACKGROUND ON PHYSICAL PROPERTIES OF NAFL's

In the NAFL description of the normal state properties of the superconducting cuprates it is the magnetic interaction between planar quasiparticles which is responsible for the anomalous spin and charge behavior. The magnetic properties of the system are specified by a dynamical spin-spin response function of fermionic origin, $\chi(\mathbf{q},\omega)$, which near a peak at $\mathbf{Q}_i$, in the vicinity of the commensurate wave vector $\mathbf{Q}=(\pi,\pi)$, takes the form

$$\chi(q,\omega)=\sum_i \frac{\chi_Q}{1+(\mathbf{q}-\mathbf{Q}_i)^2\xi^2-i\omega/\omega_{\rm sf}-\omega^2/\Delta^2}. \quad (1)$$

Here $\chi_{Q_i}\gg\chi_0$ is the magnitude of the static spin susceptibility at a (possibly) incommensurate wave vector $\mathbf{Q}_i$ near $\mathbf{Q}$, ξ is the antiferromagnetic correlation length, $\omega_{\rm sf}$ specifies the low-frequency relaxational mode (spin fluctuation), brought about by the near approach to antiferromagnetism, and Δ allows for the possible presence of a spin gap at large energies. We have assumed a system of units in which the lattice spacing $a=1$. The quasiparticle spectrum is assumed to take the tight-binding form

$$\epsilon_k=-2t(\cos k_x+\cos k_y)-4t'\cos k_x\cos k_y -2t''[\cos(2k_x)+\cos(2k_y)], \quad (2)$$

where t, t', and t'' are the appropriate hopping integrals, while the effective magnetic interaction between the planar quasiparticles is specified by

$$V_{\rm eff}(\mathbf{q},\omega)=g^2\chi(\mathbf{q},\omega). \quad (3)$$

For a given system the parameters χ_{Q_i}, ξ, and $\omega_{\rm sf}$ which determine $\chi(\mathbf{q},\omega)$ are taken from fits to NMR and inelastic neutron scattering (INS) experiments, while the effective

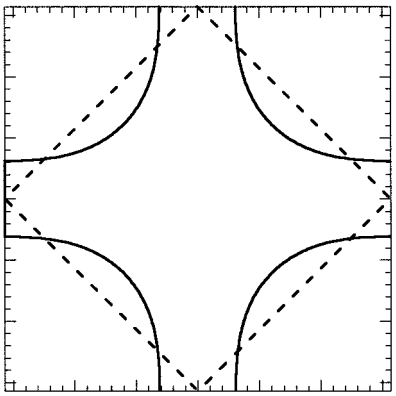

FIG. 1. A model of a Fermi surface in cuprates (solid line) and the magnetic Brillouin zone boundary (dashed line). The intercepts of two lines marks the regions of the FS near $(\pi,0)$, which can be connected by the wave vector $\mathbf{Q}_i$. These regions are most strongly scattered into each other [see Eq. (1)].

coupling constant g is assumed to be momentum independent for the wave vector near $\mathbf{Q}_i$. As discussed by Chubukov *et al.*,[29] in principle the effective interaction, Eq. (3), can be derived microscopically starting with, e.g., a one-band Hubbard model, but for a number of reasons it has not yet been possible to carry through such a derivation.

Since in practice the effective damping of the magnetic excitations is large, the term proportional to ω^2 in the denominator of Eq. (1) can be neglected, so that we may write

$$\chi(\mathbf{q},\omega)=\frac{\alpha\omega_0}{\omega_q-i\omega}, \tag{4}$$

where we have introduced the scale factor α, which relates χ_{Q_i} to ξ^2,

$$\chi_{Q_i}=\alpha\xi^2, \tag{5a}$$

$$\omega_q=\omega_{\rm sf}+\omega_0(\mathbf{q}-\mathbf{Q}_i)^2, \tag{5b}$$

and

$$\omega_0=\omega_{\rm sf}\xi^2, \tag{5c}$$

In the next section we shall for the most part assume that the spin-fluctuation spectrum possesses only a single peak at $\mathbf{Q}$; we consider, in Sec. V, the effects of incommensuration on the transport properties.

The effective interaction $V_{\rm eff}$, Eq. (3), has an obvious property: For sufficiently large correlation lengths it is highly peaked for momentum transfers in the vicinity of the antiferromagnetic wave vector $\mathbf{Q}$. The importance of this fact is hard to overestimate: If the FS of the system of fermions, defined by the quasiparticle dispersion (2), is such that it intersects the magnetic Brillouin zone Z (see Fig. 1), then quasiparticles in the vicinity of these intersection points on the FS, often referred to as hot spots,[21] are much more strongly scattered by the spin fluctuations than those which are on other parts of the FS. This is the main source of the anisotropy of quasiparticle behavior in this model, since the temperature variation of the quasiparticle scattering rates at and far away from hot spots is in general very different. We shall return to this point in the following section.

TABLE I. Crossovers temperatures and spin fluctuation parameters for representative cuprates.

	T_c	T_*	$T_{\rm cr}$ (K)
$La_{1.9}Sr_{0.1}CuO_4$	33	50	$\geqslant 500$
$La_{1.85}Sr_{0.15}CuO_4$	39	85	325
$La_{1.8}Sr_{0.2}CuO_4$	30	75	120
$La_{1.76}Sr_{0.24}CuO_4$	25	35	100
$YBa_2Cu_3O_{6.63}$	60	180	$\geqslant 600$
$YBa_2Cu_4O_8$	80	210	475
$YBa_2Cu_3O_7$	90	110	150

Barzykin and Pines (BP) have utilized Eq. (1) in their analysis[28] of the NMR results in HTS's. Because their work, subsequently extended to an analysis of INS results,[32] provides an important insight into the morphology of the magnetic spectrum in these materials, we briefly review their main conclusions. BP find that for underdoped systems low-frequency magnetic behavior possesses three distinct temperature regimes, with a crossover at $T_{\rm cr}$ from nonuniversal mean-field (MF) behavior with dynamical exponent $z=2$ to $z=1$ pseudoscaling (PS) behavior. For $T\geqslant T_{\rm cr}$, $\omega_{\rm sf}\sim 1/\xi^2$, and the product, $\chi_{Q_i}\omega_{\rm sf}\sim\omega_{\rm sf}\xi^2=\omega_0$ is independent of temperature, while between $T_{\rm cr}$ and T_*, it is $\omega_{\rm sf}\xi$ which is independent of temperature. NMR experiments show that above $T_{\rm cr}$, in the MF regime, $\omega_{\rm sf}$ and ξ^2 scale linearly with T, i.e., $\omega_{\rm sf}=A+BT$, while between T_* and $T_{\rm cr}$, the PS regime, it is $\omega_{\rm sf}$ and ξ^{-1} which scale linearly with T, albeit with a somewhat different slope and intercept of $\omega_{\rm sf}$ than that found above $T_{\rm cr}$. At $T_{\rm cr}$, the temperature-dependent uniform susceptibility $\chi_0(T)$ possesses a maximum, while $\xi\sim 2$, as has now been verified experimentally for $YBa_2Cu_3O_{6.92}$, $YBa_2Cu_4O_8$, and $La_{2-x}Sr_xCuO_4$ compounds.[32] Below T_*, in the pseudogap (PG) regime, ξ becomes independent of temperature while $\omega_{\rm sf}$, after exhibiting a minimum near T_*, rapidly increases as $1/T$ as T decreases toward T_c. In addition to the change in the magnetic fluctuation spectrum, the PS regime is characterized by a strong temperature variation of the quasiparticle band structure, resulting in a FS evolution.[29] This evolution has nontrivial consequences for the transport, as discussed in the next section.

From a magnetic perspective, the so-called optimally doped systems (e.g., $YBa_2Cu_3O_{6.93}$ and $La_{1.85}Sr_{0.15}CuO_4$) are a special case of the underdoped systems, in which T_* is comparatively close to T_c. As may be seen in Table I, $T_{\rm cr}$ varies rapidly with doping, and approaches T_c as the system approaches the overdoped regime, while T_*, which varies relatively weakly with doping, possesses a shallow maximum ($\sim$200 K in the 123 system, $\sim$100 K in the 214 system) as one varies the hole content in the planes.

From this same magnetic perspective, overdoped cuprates are defined as those for which $T_{\rm cr}<T_c$. For these systems, then, since $\xi<2$, the antiferromagnetic correlations are comparatively weak and $\chi_0(T)$ is at most weakly temperature dependent, while $\omega_{\rm sf}\propto\xi^2$ follows the linear-in-T behavior

found in the underdoped systems above T_{cr}. Examples of overdoped systems are the $T_c \sim 40$ K Tl 2212 system and $La_{2-x}Sr_xCuO_4$ for $x \geq 0.2$.

As we shall see, the crossovers seen in the low-frequency magnetic behavior possess to a remarkable extent their charge counterparts in magnetotransport and optical experiments.

III. PERTURBATION THEORY APPROACH

In this section we estimate the transport coefficients in NAFL's using a simple perturbation theory. We calculate the scattering rates for quasiparticles near the FS, assuming the effective interaction $V_{\rm eff}$, Eq. (3), and then use these to calculate the longitudinal and Hall conductivities. We discuss the behavior of these quantities in the relevant doping and temperature regimes.

Within the Boltzmann-Bloch formalism the relaxation rate for a particle near the FS is generally given by[33]

$$\frac{1}{\tau_k} = \int \frac{d^2k'}{(2\pi)^2} M(\mathbf{k},\mathbf{k}')(1-\Phi_{k'}/\Phi_k), \tag{6}$$

where Φ_k is the quasiparticle distribution function displacement obtained by solving the linearized Boltzmann equation. To second order in the coupling constant the scattering rate between points $\mathbf{k}$ and $\mathbf{k}'$ is given by

$$M(\mathbf{k},\mathbf{k}') = 2g^2 \mathrm{Im}\chi(\mathbf{k}-\mathbf{k}', \epsilon'-\epsilon)[n(\epsilon'-\epsilon)+f(\epsilon')], \tag{7}$$

where $\epsilon \equiv \epsilon(\mathbf{k})$, $\epsilon' \equiv \epsilon(\mathbf{k}')$, and $n(\epsilon)$ and $f(\epsilon)$ are the Bose and Fermi distribution functions, respectively. Note that Eq. (7) is obtained by summing the Matsubara frequencies and assuming a retarded scattering potential.[34] No lifetime effects are included. One can, of course, easily add the self-energy corrections to the bare band spectrum ϵ_k, but the lifetime effects are considerably harder to include and in principle should be obtained self-consistently. In the relaxation time approximation one replaces Φ_k, the quasiparticle distribution displacement, by $\varphi(T)(\mathbf{v}\cdot\mathbf{n})$, where φ is a function of temperature, independent of $\mathbf{k}$. The assumption that φ does not vary greatly in the Brillouin zone is most certainly invalid for HTS's,[31] given the strong momentum dependence of the effective interaction $V_{\rm eff}$, Eq. (3). However, it is still quite reasonable, as long as the temperature dependence of φ is the same in each of the hot spots, which is almost always the case. Since the inclusion of $(\mathbf{v}\cdot\mathbf{n})$ produces only a *geometric* factor (vertex correction), which is large mostly for small momentum transfer, and no additional temperature dependence, we can approximate the relaxation rate by the scattering rate, which, in the second-order Born approximation, reads

$$\frac{1}{\tau_k} = \int \frac{d^2k'}{(2\pi)^2} M(\mathbf{k},\mathbf{k}'). \tag{8}$$

One can make a change of variables in the integral in Eq. (8),

$$\int d^2k' \rightarrow \int d\epsilon' \int \frac{ds'}{|\mathbf{v}|}, \tag{9}$$

and solve the integral over ϵ' analytically for $\mathbf{k}$ near the FS ($\epsilon \approx 0$) using

$$\int dx n(-x) \frac{-x}{\Omega^2+x^2} f(x) = \frac{\pi}{2\Omega} + \pi \sum_n \frac{(-1)^n}{\Omega + n\pi} = \frac{\pi}{2\Omega} - h\left(1+\frac{\Omega}{\pi}\right), \tag{10}$$

where

$$h(x) = \frac{1}{2}\left[\psi\left(\frac{x+1}{2}\right) - \psi\left(\frac{x}{2}\right)\right], \tag{11}$$

which has the following limiting behavior:

$$h(1+x) \approx \ln 2 - \frac{\pi}{2}x, \quad x \rightarrow 0, \tag{12}$$

$$h(x) \approx \frac{1}{2}\frac{1}{x+1}, \quad x \rightarrow \infty. \tag{13}$$

Thus the integral in Eq. (10) can be approximated by

$$\frac{\pi}{2}\left(\frac{1}{\Omega} - \frac{1}{\Omega+\pi}\right) \tag{14}$$

and the scattering rate, Eq. (8), is given by

$$\frac{1}{\tau_k} = \frac{\alpha g^2 \omega_0}{4} \int_{\rm FS} dk' \tilde{M}(k,k'), \tag{15}$$

where

$$\tilde{M}(k,k') = \frac{1}{|\mathbf{v}|} \frac{T^2}{\omega_{kk'}(\omega_{kk'}+\pi T)}. \tag{16}$$

Note that in a typical FL one has an identical expression; however, $\omega_{k,k'}$ is large, temperature independent, and only weakly dependent on $\mathbf{k},\mathbf{k}'$. Then for $T \ll \omega_{kk'}$ the scattering rate has the usual T^2 temperature dependence which ceases only when $T \sim \omega_{k,k'}$. In a realistic metal, however, this energy scale can be considerably reduced for certain $\mathbf{k}$ due to the presence of band singularities at these points. In a NAFL, however, $\omega_{k,k'}$ is a strong function of momentum transfer $\mathbf{q}$; i.e., $\omega_{k,k'}$ has a minimum for $\mathbf{q}=\mathbf{Q}$. Thus, the scattering rate $\tilde{M}$ is maximized for points $\mathbf{k}$ and $\mathbf{k}'$ on the FS such that $\mathbf{q}=\mathbf{k}-\mathbf{k}'=\mathbf{Q}$.

We now calculate the scattering rate for a quasiparticle near the FS as a function of T and Δk, where Δk is the distance to a nearby hot spot along the FS. For the commensurate case and a large FS the hot spots are usually distributed along the FS in such a way that one can write, for $\mathbf{k}-\mathbf{k}' \approx \mathbf{Q}$, that $(\mathbf{k}-\mathbf{k}'-\mathbf{Q})^2 \approx (\Delta k)^2 + (\Delta k')^2$, where Δk and $\Delta k'$ are the displacements of $\mathbf{k}$ and $\mathbf{k}'$ from the nearby hot spots (see Fig. 1) (the adjoint hot spots correspond to $\Delta k, \Delta k' = 0$). This basically means that there is no strong nesting at $\mathbf{q} \approx \mathbf{Q}$, and the FS and its shadow FS, obtained by translating the FS by $\mathbf{Q}$, intercept at a high angle $\Omega \sim \pi/2$. Then one easily finds

$$\frac{1}{\tau_k}=\frac{\alpha g^2 T\sqrt{\omega_0}}{4v_f}\left(\frac{1}{\sqrt{\omega_{\rm sf}+\omega_0(\Delta k)^2}}-\frac{1}{\sqrt{\omega_{\rm sf}+\pi T+\omega_0(\Delta k)^2}}\right), \tag{17}$$

where we have assumed that the integration over $\Delta k'$ in Eq. (16) can be extended to infinity. Equation (17) can be rewritten as

$$\tau_k=\frac{4v_f Q_k}{\alpha\pi g^2 T^2\sqrt{\omega_0}}, \tag{18}$$

where

$$Q_k=\sqrt{\omega_{\rm sf}[1+(\xi\Delta k)^2]}\sqrt{\omega_{\rm sf}[1+(\xi\Delta k)^2]+\pi T} \times\{\sqrt{\omega_{\rm sf}[1+(\xi\Delta k)^2]}+\sqrt{\omega_{\rm sf}[1+(\xi\Delta k)^2]+\pi T}\}. \tag{19}$$

Note that this result is easily generalized to arbitrary Ω by replacing Δk with $(\Delta k)\sin\Omega$.

Before proceeding with the transport coefficients it is instructive to calculate the scattering rates for different values of Δk. Equation (19) suggests that there are primarily two regions of interest: We call a region of momenta k hot if

$$\Delta k\leqslant 1/\xi, \tag{20}$$

and we call a region cold if

$$\Delta k\geqslant 1/\xi. \tag{21}$$

Clearly the relaxation times in these two regions are different. In the hot region one has

$$Q_k\approx\sqrt{\omega_{\rm sf}}\sqrt{\omega_{\rm sf}+\pi T}(\sqrt{\omega_{\rm sf}}+\sqrt{\omega_{\rm sf}+\pi T}). \tag{22}$$

The fits to NMR experiments of Barzykin and Pines[28] show that in all HTS's one can assume for practically all temperatures of interest that, to a good approximation,

$$\omega_{\rm sf}\ll\pi T, \tag{23}$$

and hence in the hot region we have

$$\frac{1}{\tau_k}\approx\frac{\alpha g^2 T\xi}{4v_F}. \tag{24}$$

On the other hand, in the limit $\xi\gg 1$, in the cold region one has

$$Q_k\approx\sqrt{\omega_0(\Delta k)^2}\sqrt{\pi T+\omega_0(\Delta k)^2} \times[\sqrt{\omega_0(\Delta k)^2}+\sqrt{\pi T+\omega_0(\Delta k)^2}]. \tag{25}$$

Here we distinguish two different cases, depending on the value of Δk, yielding

$$\frac{1}{\tau_k}=\frac{\alpha g^2 T}{4v_f(\Delta k)},\quad \pi T\gg\omega_0(\Delta k)^2, \tag{26}$$

$$\frac{1}{\tau_k}=\frac{\alpha\pi g^2 T^2}{8v_f(\Delta k)^3\omega_0},\quad \pi T\ll\omega_0(\Delta k)^2. \tag{27}$$

Obviously, the scattering rates depend on the particular temperature regime for the magnetic fluctuations, through the temperature dependence of $\omega_{\rm sf}$ and ω_0. In the $z=2$ MF regime $\omega_0=\omega_{\rm sf}\xi^2=$const and $\omega_{\rm sf}=A+BT$, and therefore it is easy to verify [see Eq. (19)] that the behavior of the scattering rate for any Δk can be obtained from the $\Delta k=0$ case by replacing A in $\omega_{\rm sf}$ with $A+\omega_0(\Delta k)^2$. In other words, every point on the FS has a similar shape of $1/\tau_k$; the hot region is enlarged with increasing temperature, as can be verified from Eq. (21).

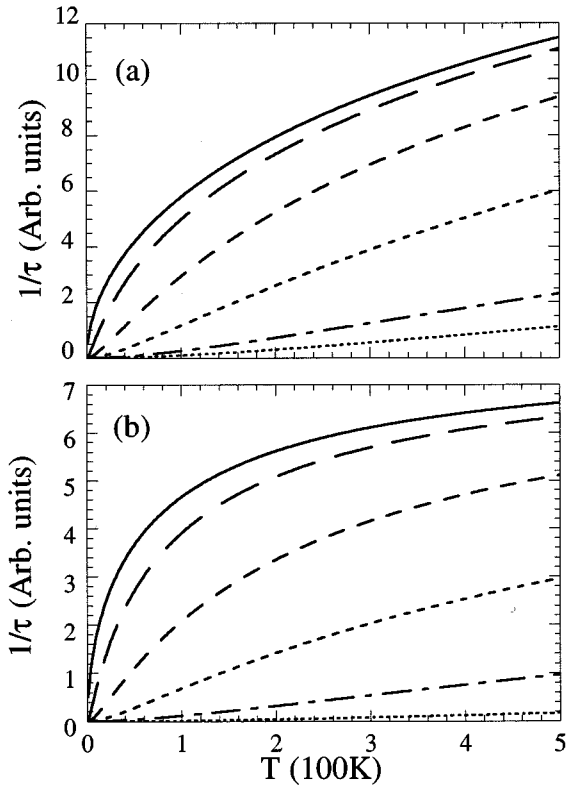

FIG. 2. Scattering rates, in arbitrary units, as a function of T in the mean-field $z=2$ regime, for several values of Δk, the displacement of the wave vector k from a hot spot. In both plots we have assumed $\omega_{\rm sf}=0.2T$, $\omega_0=600$ K. The curves correspond to (top to bottom) $\Delta k=0$, 0.1, 0.25, 0.5, 1, and 2. Panel (a) shows the case of a quite *large* FS, $\Delta k_{\rm max}=2$, and panel (b) that of a typical small one, $\Delta k_{\rm max}=0.5$.

In the $z=1$ PS regime the situation is somewhat different, due to the temperature dependence of ω_0, $\omega_0\sim 1/T$. First, from Eq. (24) it is clear that the scattering rate due to spin-fluctuation scattering is roughly temperature independent in the hot region. The scattering rate in Eq. (26), valid for $\xi\Delta k\ll\sqrt{\pi T/\omega_{\rm sf}}$, is applicable in this case as well. Finally, far away from hot spots, Eq. (27), the scattering rate is proportional to T^3. Note that the condition $\omega_0(\Delta k)^2\gg\pi T$ is satisfied for significant portions of the FS at very low temperatures. The scattering rates as functions of temperature for several different values of Δk, in the MF and PS regimes, are given in Figs. 2(a) and 3(a).

In the PG case the situation is even more complicated and somewhat unclear, due to the FS evolution mentioned in Sec. II. Here Δk does not correspond to a fixed point on the FS, since the FS itself migrates with decreasing temperature. Nevertheless, provided that the FS is still relatively large, the scattering rates are nominally the same as in the PS case,

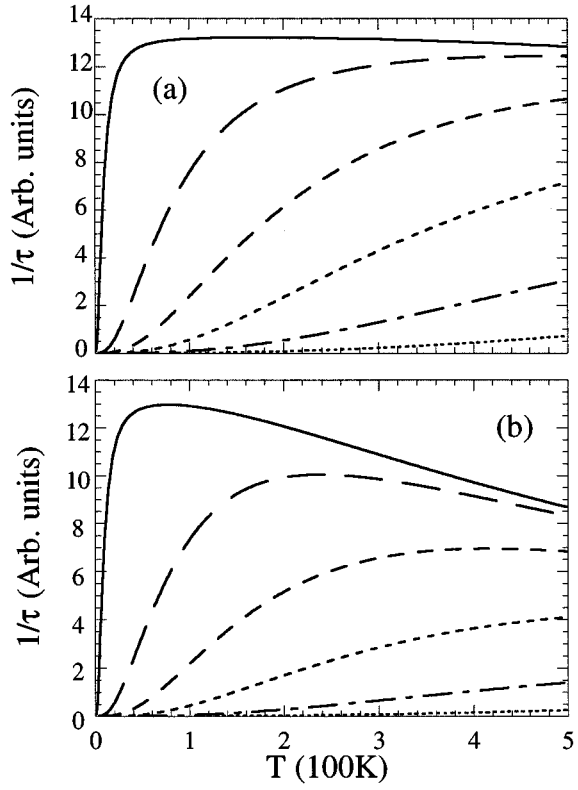

FIG. 3. Scattering rates, in arbitrary units, as a function of T in the pseudoscaling $z=1$ regime, for several values of Δk, the displacement of the wave vector k from a hot spot. In both plots we have assumed $\omega_{sf}=0.2T$, $\omega_0=1000$ K/T and the curves correspond to (top to bottom) $\Delta k=0$, 0.1, 0.25, 0.5, 1, and 2. Panel (a) shows the case of a *large* FS, $\Delta k_{max}=2$, and panel (b) that of a small one, $\Delta k_{max}=0.5$.

since $\omega_0=\omega_{sf}\xi_c^2\sim 1/T$, where $\xi_c\sim$const is the correlation length at T_c and $\omega_{sf}\sim 1/T$. However, the scattering rate at a particular point in the Brillouin zone is nontrivial and we do not present it here.

So far we have neglected the fact that in deriving Eq. (17) the integral over $\Delta k'$ was performed from $(-\infty,\infty)$. This is quite reasonable provided that the system is far from the PG regime. However, as mentioned in Sec. II, as the temperature is lowered toward T_* the quasiparticle spectral weight is removed from the hot spots due to strong spin-fermion vertex corrections and at $T\sim T_*$ the system actually starts to lose parts of the FS. Hence, one must assume a finite limit of integration over $\Delta k'$, yielding a somewhat more cumbersome form of Eq. (17) which we do not quote here. However, it is straightforward to show that although this does not affect the cold regions very much, the scattering rate in the hot region is considerably modified, as shown in Figs. 2(b) and 3(b). Although somewhat surprising, this result is natural in view of the FS modulation: The hot spots migrate with decreasing temperature and the effective size of the FS is reduced, thereby reducing the scattering of quasiparticles in the magnetic channel. More importantly, since the FS is small—i.e., Δk_{max} is very small—the scattering is anomalous around most of the FS, as can easily be verified from Eq. (19). We return to this point shortly.

The low-field longitudinal and Hall conductivities are calculated according to

$$\sigma_{xx}=-2e^2\sum_k (\mathbf{v_k}\cdot\mathbf{n})^2\tau_k\left(\frac{\partial f_0}{\partial\epsilon}\right), \tag{28}$$

$$\sigma_{xy}=-2e^3\sum_k (\mathbf{v_k}\cdot\mathbf{n}_\perp\tau_\mathbf{k})\mathbf{v}_k\times\mathbf{B}\cdot\nabla(\mathbf{v_k}\cdot\mathbf{n}\tau_k)\left(\frac{\partial f_0}{\partial\epsilon}\right), \tag{29}$$

where $\mathbf{n}$ and $\mathbf{n}_\perp$ are unity vectors perpendicular to the applied electrical field E and $\mathbf{B}$ is the applied transverse magnetic field.

We start with the resistivity. At relatively low temperatures $T\ll E_F$, where E_F is the Fermi energy, one can perform the change of variables (9) and integrate over ϵ. Assuming that the FS is fourfold symmetric (tetragonal symmetry), the conductivity is given by

$$\sigma_{xx}=\frac{e^2}{4\pi^2}\int_{\mathrm{FS}} dk\,\tau_k v_f. \tag{30}$$

Assuming that the Fermi velocity does not vary appreciably around the FS, we find that the conductivity is roughly proportional to the average of the scattering time (18) around the FS. From Eq. (18) it is clear that the main contribution to the conductivity comes from the cold regions of the FS where τ_k is the largest, while the hot spots ($\Delta k\sim 0$) contribute relatively little. On averaging Eq. (19) we obtain, at low temperatures, a simple analytic result

$$\rho_{xx}\approx\frac{\alpha g^2\pi}{v_f}\frac{T^2}{T_0+T}\frac{1}{(\Delta k_{max})^2} \tag{31}$$

up to the logarithmic corrections of order $\ln(\omega_0/\pi T)$. Here T_0 is a crossover temperature given by

$$T_0\approx\omega_0(\Delta k_{max})^2/2\pi\equiv(\xi\Delta k_{max})^2\omega_{sf}/2\pi, \tag{32}$$

where Δk_{max} is the distance between a cold spot (defined as those points on the FS which are maximally distant from a hot spot) and the nearest hot spot. As is evident from Eq. (32), T_0 depends on both the underlying spin dynamics, through ξ and ω_{sf}, and on the quasiparticle band structure. As may be seen in Fig. 1, the size of the Δk_{max} is related to the departure of the FS from the magnetic Brillouin zone boundary. For this FS and any large FS, such as is found by ARPES measurements for $YBa_2Cu_3O_7$ and related compounds, $\Delta k_{max}\sim 1$. On the other hand, for a small doping level or in the presence of substantive incommensuration (which increases the number of hot spots and acts to reduce significantly the distance between hot and cold spots), one finds $\Delta k_{max}\leqslant 0.3$.

The energy scale T_0 is a central quantity in our theory of charge dynamics. Above T_{cr} it is independent of temperature, while below T_{cr} it depends on temperature through the variation of both ω_{sf} and ξ, as well as temperature dependence of Δk_{max}. Numerically, it can be as low as 1 meV in underdoped materials, for which Δk_{max} is very small, so that for such systems a linear-in-T resistivity can persist down to very low temperatures. On the other hand, T_0 can be as high

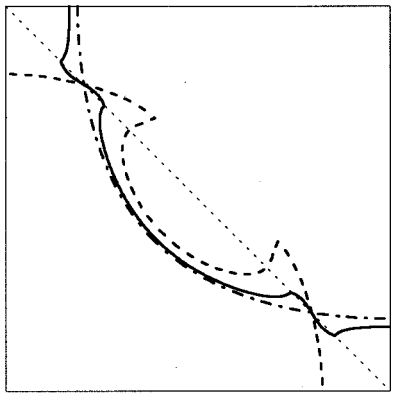

FIG. 4. The FS as a function of coupling constant g in a NAFL. The figure shows only one quarter of the Brillouin zone. The curves are obtained using the same formalism and the same values of spin fluctuation and band parameters as in Ref. 35. The dash-dotted, solid, and dashed lines correspond to increasing values of g. As shown in Ref. 29, these curves also correspond to high, intermediate, and low temperatures, respectively. Note that the effect of the interaction is to move the FS towards the magnetic Brillouin zone boundary (here depicted by the dotted line). Hence the interaction effectively reduces $\Delta k_{\max}$.

as 50 meV in the overdoped materials with large FS's, yielding a FL-like resistivity up to relatively high temperatures.

It is evident from Eq. (31) that in the absence of any evolution of the Fermi surface with temperature, ρ_{xx} will be linear in temperature as long as T is appreciably greater than T_0. As noted above, in the MF regime, T_0 is independent of temperature, while in the PS regime it increases as $\xi(\sim 1/T)$ as T decreases. If $\Delta k_{\max}$ and $\xi(T_*)$ are small enough, then $T_0 \leqslant T_*$, and the resistivity will be linear-in-T down to T_*. The exact condition for this extended linear in T behavior reads $(\Delta k_{\max})^2 \xi(T_*) \leqslant (T_*/\hat{c})$, where $\hat{c}$ is the pseudoscaling spin velocity, $\omega_{\rm sf}\xi$. Under these circumstances, any change in ρ_{xx} at $T_{\rm cr}$ will be marginal, since it can only arise from changes in the *hot* region contribution to ρ_{xx}. The linearity in T continues above $T_{\rm cr}$ until $T \sim \omega_0$, an experimentally almost unreachable temperature. Moreover, we have assumed that the only relevant scattering is in the magnetic channel. Strictly speaking, in addition to the contribution proportional to χ defined above one must add the FL contribution $\chi_{\rm FL}$, present in all FL's, to the effective interaction $V_{\rm eff}$. The latter is likely to dominate at these temperatures. Without this term at $T > \omega_0$ one then has $\rho_{xx} \propto T^{1/2}$, provided $\omega_{\rm sf} \propto T$. On the other hand, from Eq. (19) it is readily shown that if $\omega_{\rm sf} \approx$ const, then $\rho_{xx} \propto T^2$. We shall return to this point when discussing overdoped samples.

What happens at T_*? As mentioned in Sec. II, in the vicinity of T_* the quasiparticle band structure begins to acquire a considerable temperature dependence, implying a FS evolution as well. Recently, Chubukov, Morr, and Shakhnovich[35] studied the FS evolution as a function of the coupling strength g at $T=0$ and found that with increasing spin-fermion interaction the FS acquires features of a preformed spin-density-wave state, as depicted in Fig. 4. Alternatively one can show[29] that a similar evolution occurs at fixed g, but as a function of temperature, associated with a relatively strong temperature dependence of the spin-fluctuation damping.[29] As a result, the FS appears to get closer to the magnetic Brillouin zone boundary—i.e., the effective size of the FS decreases—with decreasing temperature. Hence when calculating transport coefficients one should assume that $\Delta k_{\max}$ acquires a temperature dependence, the precise form of which is not well known at present. Below T_* one finds that ω_0 retains its $1/T$ overall temperature dependence although it changes its slope: ξ becomes constant, while $\omega_{\rm sf}$ increases as T^{-1}. Whether one gets a crossover at T_0 in the PG regime will then depend sensitively on the interplay between $\Delta k_{\max}(T)$ and $\omega_{\rm sf}(T)$. If a crossover to $\rho_{xx} \propto T^2/T_0$ occurs, the resistivity will then decrease faster than T^2, due to the temperature dependence of T_0.

Let us examine the crossover in the vicinity of T_* in more detail. The above-mentioned FS evolution usually closes channels for scattering as the temperature is lowered below T_*. New hot spots are developed and a smaller portion of the FS is now *cold*. At the same time ω_0 is strongly temperature dependent in both PS and PG regimes. Assuming that $T \gg T_0(T)$ above T_* the reduction in size of the cold region implies that a large part of the FS has a scattering rate such as those shown in Fig. 3 for small values of Δk, where $1/\tau$ is roughly independent of T. At a certain temperature T_*^r the FS is effectively so small that the quasiparticles around most of the FS exhibit precisely these (almost constant in T) scattering rates; the resistivity thus acquires a finite negative curvature, i.e., $d^2\rho_{xx}/dT^2 < 0$. A signature of this should be seen in the T variation of the scattering rate at a hot spot $\Delta k \sim 0$. In the next section we shall see that this is indeed the case. It is important to realize that this can occur only when ω_0 is strongly temperature dependent; hence T_*^r is never larger than $T_{\rm cr}$, where $\omega_0 =$ const, although in principle it can be comparable to $T_{\rm cr}$. A rapid temperature dependence of ω_0 eventually leads to a Fermi-liquid-like behavior at $T \ll T_*^r$, regardless of the precise size of the FS. Note that perturbation theory is only marginally applicable in the PG regime, since one must include the strong vertex corrections at or near hot spots, although the fact that the conductivity is dominated by regions away from hot spots, where the above corrections are not as pronounced, allows us to make this qualitative argument. We note that the present theory is somewhat equivalent to the work of Levin and Quader,[18] although in their case the scattering channels which open up at T_*^r are attributed to the multiband structure in bilayer cuprates and the proximity of one of the bands to the Fermi level.

Overdoped materials exhibit only $z=2$ scaling and in general $\omega_{\rm sf}$ and ξ show very little T dependence. Quite generally in overdoped samples $\omega_{\rm sf} = A + BT$ displays a much larger value of A, associated with the strong fermionic damping of the spin fluctuations, found at high doping levels. Hence, even at a hot spot ($\Delta k = 0$) the scattering rate $1/\tau_k$ is only weakly anomalous, i.e., $1/\tau_k \sim T$ or even T^2. Therefore in the overdoped samples one encounters a crossover from quadratic-in-T behavior of the resistivity to linear-in-T behavior above T_0, even though the amount of the anomaly in the hot regions is weak. However, there are extreme cases, such as the overdoped samples of 214 ($x \geqslant 0.25$), where the anomalous behavior is so weak that the resistivity is never

TABLE II. The transport coefficients in various temperature regimes.

	σ_{xy}	ρ_{xx}	ρ_{xy}	$\cot\Theta_H$
$T<T_0$	T_0/T^4	T^2/T_0	const	T^2/T_0
$T_0<T<2\pi T_0$	T_0/T^3	T	T_0/T	T^2/T_0
$T>2\pi T_0$	$1/T^2$	T	const	T

linear in T. Moreover, in overdoped materials both the large values of $\omega_{\rm sf}$ and the small values of ξ imply that the anisotropy of scattering rates in overdoped materials is seriously reduced [see Eq. (19)], producing only a weakly temperature-dependent Hall coefficient.

We now turn to the Hall effect. Here the situation is, in principle, a lot trickier, since the Hall coefficient is a nontrivial function of temperature, due to the strong anisotropy of the mean free path, $\ell\equiv\tau_k v_k$, as readily observed from the definition of σ_{xy} [Eq. (29)]. However, in practice complications occur only if ℓ has a very peculiar periodicity as k goes around the FS. For the FS's seen in ARPES measurements on a number of samples near optimal doping one can safely assume

$$\sigma_{xy}=\frac{e^3B}{4\pi^2}\int_{\rm FS}dk\ell_k^2, \tag{33}$$

where we have performed an integration over ϵ in Eq. (29) in the usual manner. Again, assuming that v_f does not vary appreciably around the FS, one concludes that σ_{xy} is roughly proportional to the average of τ_k^2. Clearly, the leading contribution to this quantity comes from the regions of the FS where $\Delta k\sim\Delta k_{\rm max}$ (cold regions); the hot regions contribute very little. On averaging τ_k^2 over Δk [Eq. (19)], we make the same approximations as before, i.e., $\omega_{\rm sf}\ll\pi T$ and $\Delta k\xi\gg 1$ in the cold regions of interest. The result for σ_{xy} is again cumbersome, but can be simplified by expanding $\sigma_{xy}T^4$ in T, leading to a relatively simple formula

$$\sigma_{xy}\approx\frac{e^3Bv_f^2}{4\alpha^2g^4\pi^2}\frac{(\Delta k_{\rm max})^3}{T^4}(3T_0^2+6T_0T+T^2/\sqrt{2}), \tag{34}$$

where T_0 is defined in Eq. (32). Equation (34) is valid over an extended temperature range. Clearly, through the variations in T_0 and $\Delta k_{\rm max}$, it leads to a rather complex morphology of the Hall effect.

Our result, Eq. (34), suggests that there are three temperature regimes for the Hall effect in NAFL's: In the low-temperature regime $\sigma_{xy}\propto T_0^2/T^4$ and in the high-temperature regime $\sigma_{xy}\propto 1/T^2$, while at the intermediate temperatures $\sigma_{xy}\propto T_0/T^3$. The exact values of the crossover temperatures depend greatly on the details of the band structure. In what follows we shall assume, for the purpose of simplicity, that the crossover between the low- and intermediate-temperature regimes occurs at T_0 and that the crossover between intermediate and high temperatures occurs at $2\pi T_0$, where T_0, given by Eq. (32), is the crossover temperature observed in the resistivity; the estimate of other quantities, such as the Hall coefficient, is then rather convenient. Our results for the transport coefficients are given in Table II. Note that for many systems away from the PG regime one finds $\cot\Theta_H\sim T^2$, due to the relatively large value of the second crossover temperature T_2.

Our discussion of the resistivity in underdoped cuprates is easily extended to σ_{xy}: In the MF regime T_0 is constant and hence

$$\sigma_{xy}\sim T^{-3}, \tag{35a}$$

$$\cot\Theta_H\sim T^2, \tag{35b}$$

$$\rho_{xy}\sim 1/T, \tag{35c}$$

for temperatures well below $\omega_0(\Delta k_{\rm max})^2$. At somewhat higher temperatures the second crossover in σ_{xy} is approached so that both ρ_{xy} and $\cot\Theta_H$ deviate from this behavior. In the PS regime $\sigma_{xy}\propto T_0/T^3$, decreases faster than $1/T^{-3}$, since T_0 decreases with temperature. As T approaches $T_{\rm cr}$ one finds $\sigma_{xy}\sim T^{-3}$ even in this regime. Note that in this case the Hall coefficient varies faster than $1/T$. Finally, due to the variation of T_0, the second crossover can be approached, in which case ρ_{xy} becomes only weakly temperature dependent. We emphasize once more that in both MF and PS regimes the results depend a great deal on details of the band structure. Moreover, the presence of impurities makes a nontrivial effect on all of the quantities of interest.

As before the PG regime is even more complex due to the very rapidly varying ω_0 and the FS evolution, which alters $\Delta k_{\rm max}$. Although it is not clear what the temperature dependence of T_0 is in this case, due to the fact that at present one does not know the temperature variation of the band structure in detail, we can still make certain arguments. Near T_* the value of T_0 changes rapidly and one can easily switch between several regimes, due to the sensitivity of the Hall effect to the variation in the band structure. For example, one can jump from the first (low-T) regime to the third, without noticing a substantial difference in, e.g., the Hall coefficient, since in both cases the quantity is roughly constant, while σ_{xx} and σ_{xy} both experience nontrivial changes. Finally, at very low temperatures one finds ρ_{xy} approximately constant and $\cot\Theta_H$ varying faster than T^2.

The NAFL model suggests a very complex morphology of the transport coefficients in HTS's. We explore the extent to which this morphology is experimentally supported in the next section.

IV. ANALYSIS OF TRANSPORT MEASUREMENTS

In this section we review briefly the in-plane normal state transport properties of the cuprate superconductors, with particular attention to the extent to which the doping and temperature dependence of the planar resistivity ρ_{xx} and the Hall conductivity σ_{xy} reflect the magnetic crossovers discussed in Sec. II and the perturbation theoretic estimates of scattering rates given in Sec. III. We then use a phenomenological model which incorporates the expected highly anisotropic quasiparticle mean free path to deduce from experiments the detailed behavior of the quasiparticle scattering rates in both the hot and cold regions of the Fermi surface. We focus on the results obtained for the bilayer 123 system (of which $YBa_2Cu_4O_8$, whose behavior corresponds closely to that found in $YBa_2Cu_3O_{6.68}$, is an ''honorary'' member), the

single-layer $La_{2-x}Sr_xCuO_4$ (214) system, and, as representative of overdoped materials, the 15-K single-layer Tl 2201 material.

It is often stated that optimally doped materials, such as $La_{1.85}Sr_{0.15}CuO_4$ and $YBa_2Cu_3O_{6.93}$, possess a resistivity which is linear in T over a wide temperature region which extends down to T_c. However, close examination of single-crystal data shows that as T approaches T_*, departures from linearity occur in these materials, departures which are in fact characteristic of all underdoped materials, but which become more pronounced as one reduces the doping level below the optimum level. Quite generally, ρ_{xx} in underdoped cuprates exhibits a drop (below linear behavior) at a temperature, T_*^r, which for many systems is not far from the temperature T_* at which the low-frequency magnetic behavior crosses over from the PS to the PG regime. On the other hand, in overdoped materials, ρ_{xx} displays an upturn (from linear behavior) with decreasing T, an upturn which we attribute to the comparatively weak anomalous scattering in the vicinity of the hot spots we have discussed in Sec. III. Thus one encounters qualitatively different departures from linearity, depending on whether one is describing a system which is overdoped or underdoped (using the magnetic classification proposed by Barzykin and Pines). Some of the experimental results which have led us to this conclusion are given in Fig. 5. We note that the transport results presented in Fig. 5(a) provide additional support for the assignment, based on analysis of NMR data,[28] of ''optimally doped'' $YBa_2Cu_3O_{6.92}$ material to the underdoped sector.

To what extent does the crossover at T_*^r correspond to the magnetic crossover at T_*? As may be seen in Fig. 5(a) and Fig. 6, for $YBa_2Cu_3O_7$ and $YBa_2Cu_3O_{6.63}$ and 124, within the present experimental uncertainties, the two crossover temperatures agree. However, the perturbation theory analysis of Sec. III suggests that this need not be the case in general, since if the FS is sufficiently far from the magnetic Brillouin zone boundary, T_*^r can be considerably higher than T_*; this appears to be the case for the underdoped members of the 214 family [see Fig. 5(b) for $La_{1.9}Sr_{0.1}CuO_4$ and Table I]. On the other hand, to our knowledge there are no samples for which T_*^r is appreciably lower than T_*.

We have called attention, in Sec. III, to the possibility of a crossover to almost Fermi-liquid-like behavior for ρ_{xx}. This occurs when $T<T_0(T)$ [see Eq. (32)]. This crossover is found in most, if not all, underdoped materials, at sufficiently low temperatures, where ρ_{xx} displays a finite positive curvature above linearity, $\rho_{xx}=\rho_{xx}(0)+\beta T^b$, with b larger than 1. Indeed, as may be seen in Fig. 7, reasonable fits to the data may be obtained with $b\sim 2$. Note that here $\rho_{xx}(0)$ is the actual residual resistivity, due presumably to disorder in a sample.

In the overdoped materials one also observes a crossover from $\rho=\rho_{xx}(0)+\beta T^2$ to linear-in-T behavior at higher temperatures, as already illustrated by the Tl 2201 result in Fig. 5(a). We emphasize once again that the physics of this crossover is different than in underdoped materials, as it arises from the fact that the anomaly of scattering at hot spots is rather weak in these compounds, rather than in the pseudogap effects found in the underdoped cuprates. It is important to notice, however, that there is no second crossover; i.e., T_*^r has not been observed. Moreover, in some overdoped materials, such as $La_{2-x}Sr_xCuO_4$ at the doping level $x=0.3$, the resistivity is never linear in T; i.e., $\rho\approx T^{3/2}$ over the entire T range.[36]

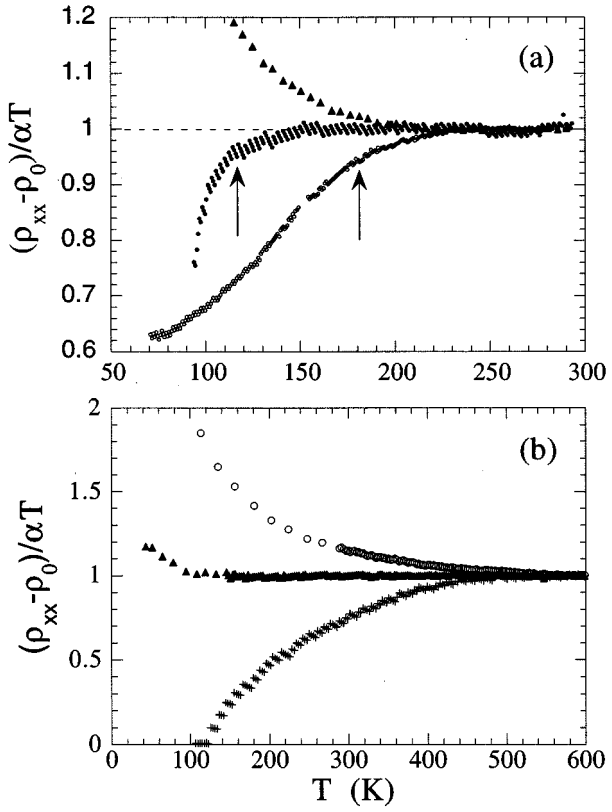

FIG. 5. The measured resistivity as a function of temperature, showing the deviation from linearity in T in underdoped, overdoped, and optimally doped cuprates. Panel (a) shows the results from Refs. 44, 45, and 46, obtained in (top to bottom) 15-K Tl 2201, $YBa_2Cu_3O_7$, and $YBa_2Cu_3O_{6.63}$ compounds. The dashed line is a guide to the eye and the arrow marks the crossover from pseudoscaling to pseudogap behavior at T_* in the underdoped and optimally doped materials. Panel (b) shows $La_{2-x}Sr_xCuO_4$ at three doping levels (top to bottom) $x=0.22$, 0.15, and 0.10 (Ref. 36). The quantity plotted is $[\rho_{xx}(T)-\rho_0]/\alpha T$, where ρ_0 and α are obtained by fitting the high-T, linear part of the resistivity.

The morphology of the resistivity is still more complex in materials with CuO chains. As may be seen in Fig. 8, where we show how ρ_{aa} and ρ_{bb} deviate from linearity in the 124 compound, chains lead to both a different magnitude and a different temperature dependence for ρ_{aa} and ρ_{bb} (see Ref. 37). Qualitatively similar results are found for optimally doped 123,[38] although the level of a-b plane anisotropy is considerably less prominent. On comparing Figs. 5 and 8 it may be seen that the temperature dependence of ρ_{aa} and ρ_{bb} in 124 resembles that found in the underdoped and overdoped cuprates, respectively. A detailed explanation of this unique behavior in terms of NAFL theory is given in Sec. V.

We consider next the Hall effect in a transverse magnetic field. In ordinary FL's one finds a Hall conductivity which is roughly proportional to the square of the longitudinal conductivity ($\sigma_{xy}\sim\sigma_{xx}\sigma_{yy}$), and as a consequence the Hall resistivity $\rho_{xy}=\sigma_{xy}/(\sigma_{xx}\sigma_{yy}-\sigma_{xy}\sigma_{yx})\approx\sigma_{xy}/\sigma_{xx}\sigma_{yy}$ is only

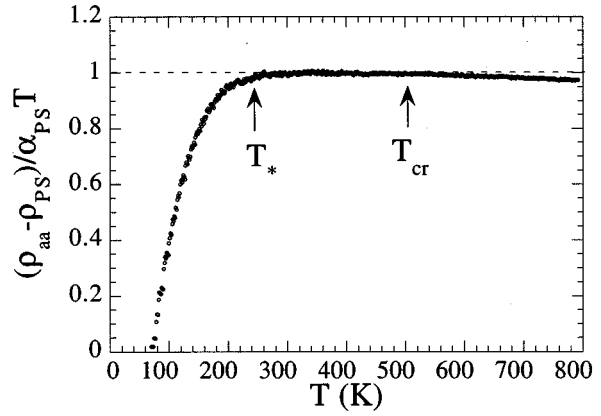

FIG. 6. The resistivity ρ_{aa}, for current running along the a crystallographic axis, as a function of T in $YBa_2Cu_4O_8$ material (Ref. 37). The quantity plotted is $[\rho_{aa}(T)-\rho_{PS}]/\alpha_{PS}T$, where ρ_{PS} and α_{PS} are obtained by fitting $\rho_{PS}+\alpha_{PS}T$ in the PS temperature regime (200 K$<T<$500 K; see Table I). The arrows mark the crossovers at T_* and T_{cr}, and the dashed line is guide to the eye. Note that ρ_{aa} retains its linearity in T above T_{cr} and that the change in slope at T_{cr} is so minor that it is dificult to detect with the naked eye.

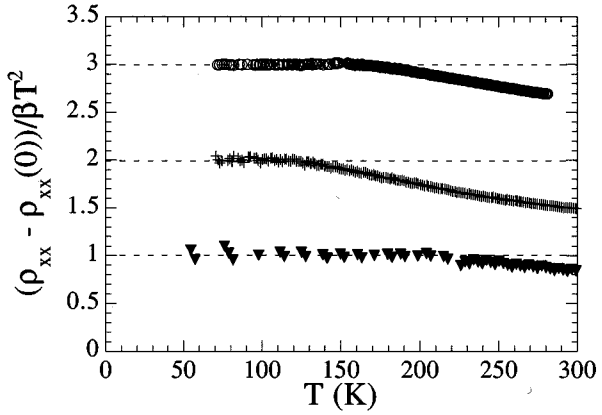

FIG. 8. The reduced resistivity $[\rho_{aa}(T)-\rho_0]/\alpha T$ in $YBa_2Cu_4O_8$ (Ref. 37) α and ρ_0 are determined as in Fig. 5. The bottom (top) set of data shows ρ_{aa} (ρ_{bb}), where ρ_{aa} (ρ_{bb}) is obtained with current running along a (b) crystallographic directions. Inset: ρ_{aa} and ρ_{bb} in $YBa_2Cu_4O_8$ material. Note that, at higher T, $\rho_{aa}\sim 3\rho_{bb}$.

weakly temperature dependent. However, this is not the case in HTS's,[38] where typically the Hall resistivity decreases sharply with increasing temperature. As discussed in the Introduction, it has been suggested [in the context of the resonating valence bond (RVB) ground state] that the scattering processes which involve ρ_{xx} and ρ_{xy} are intrinsically different, and that the cotangent of the Hall angle, $\cot\Theta_H\equiv\rho_{xx}/\rho_{xy}$, is universal and proportional to T^2 (Ref. 10). Much of the experimentally available data focus on the Hall coefficient $R_H=\rho_{xy}/B$, where B is the applied magnetic field, although the above proposal has led a number of authors to plot $\cot\Theta_H$. However, we find that an examination of the behavior of $\sigma_{xy}(T)$, a quantity more directly related to theoretical calculations, provides more insight into the underlying physical origin of the measured anomalous Hall effect behavior.

Since ρ_{xx} typically varies linearly with T for $T>T_0$, σ_{xy} must decrease faster than T^{-2} in order to bring about the temperature-dependent behavior of R_H. Examination of the experimental data presented in Figs. 9 and 10 shows that this is indeed the case at high temperatures, where σ_{xy} is seen to vary as T^{-3} for both the 123 and 214 systems. However, experiment also shows deviations from this high-temperature behavior in many systems. From Eq. (34) it is clear that if T_0 is temperature independent, σ_{xy} should indeed vary as T^{-3}. However, in the PS regime this is not the case, since $T_0\sim 1/T$ and hence the result in Fig. 9 is to some extent in contradiction with our result. However, the inset of Fig. 9 shows clearly that, in $YBa_2Cu_3O_{6.63}$, σ_{xy} obeys T^{-4} quite

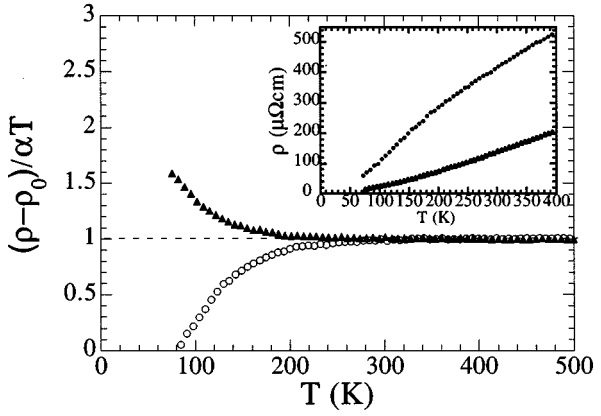

FIG. 7. $\rho_{xx}(T)$ in underdoped cuprates at low temperatures. The three sets of data are shifted by 1 for clarity and correspond to (top to bottom) $YBa_2Cu_3O_{6.68}$, $YBa_2Cu_4O_8$, and $La_{1.9}Sr_{0.1}CuO_4$ (Refs. 36, 37, and 46). The dashed lines are guides to the eye. The quantity plotted is $[\rho_{xx}(T)-\rho_{xx}(0)]/\beta T^2$, where $\rho_{xx}(0)$ and β are obtained by fitting $\rho_{xx}=\rho_{xx}(0)+\beta T^2$ at low T.

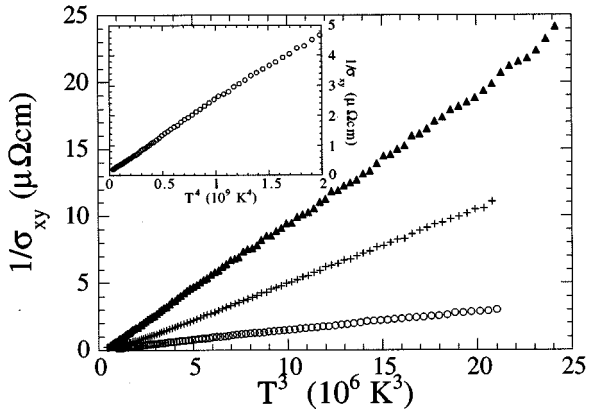

FIG. 9. The inverse Hall conductivity as a function of temperature in 123 and $YBa_2Cu_4O_8$ compounds. The data correspond to the measured results obtained in (top to bottom) $YBa_2Cu_4O_8$, $YBa_2Cu_3O_{6.63}$, and $YBa_2Cu_3O_7$ (Refs. 37, 45, and 46). Note that at sufficiently high temperature all curves satisfy T^3 quite well. Inset: the result for $YBa_2Cu_3O_{6.63}$, showing that $\sigma_{xy}\propto T^{-4}$ at low T.

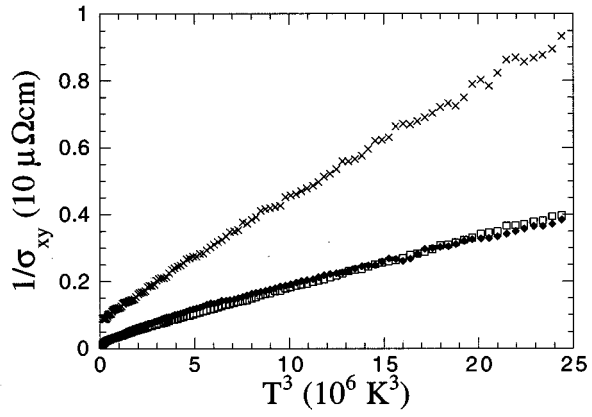

FIG. 10. The inverse Hall conductivity for the 214 compound. The data are taken from Ref. 36 and correspond to doping levels (top to the bottom) $x=0.10$, 0.15, and 0.22. The curves show large positive intercepts, suggesting a considerable amount of disorder and/or a smaller FS in this system.

well up to temperatures $T\sim 200$ K, where the first deviations from T^{-4} behavior occur. In fact, only well above this temperature does σ_{xy} become proportional to T^{-3}, in agreement with our predictions. One can observe similar deviations at other doping levels in this system. Note also that $\sigma_{xy}\sim T^{-3}$ is obtained also well above $2\pi T_0$, for $T_0\sim 1/T$ (see Table II). We draw two important conclusions. First, σ_{xy} has a crossover from T^{-4} to T^{-3} behavior, the details of which depend not only on whether one is above T_0, but also on the temperature regimes considered. Second, and more importantly, the ''disagreement'' in the experimental data in Fig. 9 and its inset shows clearly that one should not use simple-minded power law fits, as is often done in the literature, but more complex formulas like Eq. (34), which include all necessary crossovers. In addition, we note that one must be very careful when fitting to the Hall effect data, since impurities play an important role, and their presence can lead to large positive intercepts of $1/\sigma_{xy}$ as a function of T^3, such as that seen in Fig. 10. Moreover, as mentioned above, the chain contribution in various materials is nontrivial and may obscure a crossover in the in-plane Hall effect. Finally, we remind the reader that Eq. (34) is obtained in the limit $\omega_{\rm sf}\ll T$. This limit is not well satisfied in highly overdoped materials where a somewhat different sequence of crossovers may occur.

Further insight into the role played by anisotropic quasiparticle scattering may be obtained using a phenomenological model for the variation in the mean free path as one goes around the FS. For simplicity, we consider a representative FS and anisotropic quasiparticle behavior which exhibits a fourfold symmetry. We assume a cylindrical FS with approximately constant k_f, but with an anisotropic effective mass m_k. We parametrize the mean free path (MFP) by assuming that there are hot regions on the FS at 90° with respect to each other, and choose as a representative FS that depicted in Fig. 1. In the extended zone scheme this FS is approximately a large distorted circle, centered around (π,π), with hot spots near $\mathbf{k}=\pm(\pi,0)$ and $\mathbf{k}=\pm(0,\pi)$. Then the MFP around the FS is given by

$$\frac{1}{\ell(\theta)}=\frac{1}{\ell_{\rm hot}}\left[\frac{1+a\cos(4\theta)}{1+a}\right], \tag{36}$$

where the anisotropy parameter a varies between 0 and 1 ($a\approx 1$ for a highly anisotropic scattering rate and $a\approx 0$ for weak anisotropy), and $\ell_{\rm hot}$ is the MFP at a hot spot on the FS. Note that, in general, both a and $\ell_{\rm hot}$ are functions of temperature. For simplicity we shall assume $a=(1-r)/(1+r)$, where $r=\ell_{\rm hot}/\ell_{\rm cold}\equiv\ell(0)/\ell(\pi/4)$. This particular choice may not be the most suitable for an effective interaction which is sharply peaked at $\mathbf{Q}$, since for long correlation lengths, as one moves away from a hot spot, $1/\ell$ decays faster with θ than is assumed here. However, if the effective interaction (1) has incommensurate peaks in momentum space, then the anomalously scattered (hot) regions are large, $1/\ell$ is a slower function of θ, and Eq. (36) is quite reasonable approximation. Therefore, one should consider $\ell_{\rm hot}$ and $\ell_{\rm cold}$ here in a broader sense, recognizing that under certain circumstances it may not be possible to identify them with the results quoted in the previous section.

Starting from the expressions, (28) and (29) for σ_{xx} and σ_{xy}, at $T\ll t$ one can perform a change of variables and integrate over ϵ. The result for σ_{xx} is

$$\sigma_{xx}=\frac{e^2k_f}{2\pi^2}\int d\theta\ell\cos^2\theta, \tag{37}$$

where $\ell=\tau(\theta)k_f/m(\theta)$ and θ is the angle between the electrical field and $\mathbf{k}(\theta)$. On using the parametrization (36), we find

$$\sigma_{xx}=\frac{ne^2\tau_{\rm hot}}{m_{\rm hot}\sqrt{r}}=\frac{ne^2\tau_{\rm cold}\sqrt{r}}{m_{\rm cold}}, \tag{38}$$

where $n=k_f^2/2\pi$. In similar fashion the Hall conductivity is found to be

$$\sigma_{xy}=\left(\frac{e^3B}{2\pi^2}\right)\int d\theta\ell\cos\theta\left(\frac{d}{d\theta}\ell\sin\theta\right), \tag{39}$$

which leads to

$$\sigma_{xy}=\left(\frac{e^3B}{2\pi}\right)\ell_{\rm hot}^2\frac{1+r}{2r^{3/2}}=\sigma_{xx}eB\ell_{\rm hot}\frac{1+r}{2r}. \tag{40}$$

Equations (38) and (40) may be combined to yield simple expressions for the Hall coefficient and Hall angle:

$$R_H\approx\frac{\sigma_{xy}}{\sigma_{xx}^2B}=\frac{1}{en}\frac{1+r}{2\sqrt{r}} \tag{41}$$

and

$$\cot\theta_H=\frac{\sigma_{xx}}{\sigma_{xy}}=\frac{m_{\rm hot}}{eB\tau_{\rm hot}}\frac{2r}{1+r}. \tag{42}$$

Note that the above expressions depend only on the two temperature-dependent parameters r and $\ell_{\rm hot}$. These two quantities can be directly probed by measuring the Hall coefficient (41) and the resistivity $\rho_{xx}\approx\sigma_{xx}^{-1}$, since R_H depends only on r and the product $\rho_{xx}R_H$ yields $\ell_{\rm hot}$.

In the case of high anisotropy, i.e., $r\ll 1$, the above quantities take an especially simple form

$$\sigma_{xx} = ne^2 \sqrt{\frac{\tau_{\rm cold}\tau_{\rm hot}}{m_{\rm hot}m_{\rm cold}}}, \tag{43}$$

$$\sigma_{xy} = \sigma_{xx}\frac{\omega_c \tau_{\rm cold}}{2}, \tag{44}$$

$$R_H = \frac{1}{2ne}\sqrt{\frac{\tau_{\rm cold}/m_{\rm cold}}{\tau_{\rm hot}/m_{\rm hot}}}, \tag{45}$$

$$\cot\theta_H = \frac{2}{\omega_c \tau_{\rm cold}}, \tag{46}$$

where ω_c is the *cold* cyclotron frequency, $\omega_c = eB/m_{\rm cold}$. Our result, Eq. (46) for the Hall angle, provides a natural explanation of why the superconducting cuprates with a variety of different behaviors for $\rho_{xx}(T)$ often display a quite similar behavior of $\cot\Theta_H$. Note that Eq. (43) is exact for any r. It is clearly consistent with our conclusion in Sec. III that the linear-in-T resistivity in NAFL's is due to a fine balance between cold and hot regions. In addition, with the help of Eq. (27) one easily verifies that Eq. (44) is consistent with Eqs. (31) and (34).

One can use Eqs. (38)–(42) to deduce the temperature dependence of $(m/\tau)_{\rm hot}$ and $(m/\tau)_{\rm cold}$ from the experimentally measured ρ_{xx} and ρ_{xy}. Only one undetermined parameter enters into this procedure, namely, n, which in some cases can be obtained experimentally from the high-temperature limit of R_H, since in this case $r \to 1$, and the Hall coefficient is temperature independent. The quantity, $R_\infty \equiv R_H(T\to\infty)$ is well defined for many overdoped materials,[36] but has been determined for only a few underdoped materials. Whenever experimental data are not available we make the best estimate for R_∞: For example, in the 214 family we extrapolate $R_H(T)$ to $T = T_{\rm cr}$ and for the 124 material we assume R_∞ comparable to the result found for $YBa_2Cu_3O_{6.63}$ (Ref. 39), which has comparable magnetic properties. However, it is important to stress that as long as one has the correct order of magnitude for R_∞, qualitatively the results are virtually the same.

We proceed to extract quasiparticle scattering rates by fitting Eqs. (38)–(41) to the transport measurements considered above. Figure 11 shows the scattering rates for $YBa_2CuO_{6.63}$ in the cold and hot regions of the FS (in the same dimensionless units) as a function of temperature. Clearly in the hot region the scattering rate is much larger; it is approximately linear in T for $T \leqslant T_*^r \sim 200$ K, and becomes weakly T dependent at higher temperatures. As noted above, for this system $T_*^r \approx T_*$. At the same time $(m/\tau)_{\rm cold}$ barely reflects the crossover at T_*^r as may be seen in Fig. 12, although clearly both scattering rates are affected as the system approaches the PG regime. Note that these scattering rates closely resemble those shown in Fig. 3. In particular, the crossover to a constant scattering rate of $(m/\tau)_{\rm hot}$ is strikingly similar to the calculated one for $\Delta k \approx 0$, shown in Fig. 3.

The results for the 124 compound are given in Fig. 13, where we have taken ρ_{aa}, which does not include chain contribution and exhibits an in-plane resistivity resembling

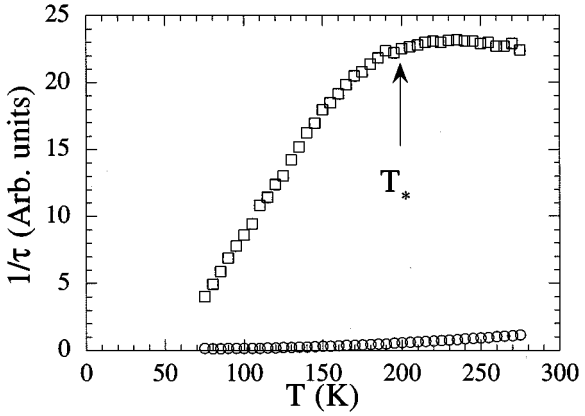

FIG. 11. The *hot* (top) and *cold* (bottom) scattering rates in $YBa_2Cu_3O_{6.68}$ in dimensionless units, obtained by fitting the results of Ito *et al.* (Ref. 46) for ρ_{xx} and ρ_{xy}, shown in the previous figures, to the phenomenological formulas (38) and (41) (see text). The rates closely resemble the calculated scattering rates shown in Fig. 3. The arrow marks the crossover at T_*.

that in underdoped materials, and used the measured values of R_H. The results are similar to those found for $YBa_2Cu_3O_{6.68}$, although in the measured temperature regime ($T < 300$ K) the scattering rate at the hot spot does not quite saturate. However, we find that, as T increases, $(m/\tau)_{\rm cold}$ becomes approximately proportional to T^2 in this material; on extrapolating this behavior of $(m/\tau)_{\rm cold}$ and the experimentally obtained resistivity, we find the same behavior of $(m/\tau)_{\rm hot}$, albeit with a somewhat higher value of $T_*^r \approx 250$ K.

Finally in Fig. 14 we show the scattering rates in the cold and hot regions for $YBa_2Cu_3O_7$: Here the scattering rate in the hot region is once more seen to saturate, but at a much lower temperature corresponding to $T_*^r \approx 120$–130 K. Both this value and that found in 124 and $YBa_2Cu_3O_{6.68}$ are very close to T_*, found by Barzykin and Pines for these materials (see Table I). Although it is not easy to verify directly in

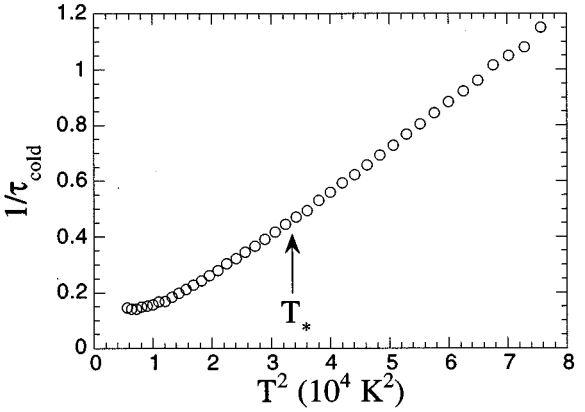

FIG. 12. The scattering rate in the cold regions of $YBa_2Cu_3O_{6.68}$ obtained from experimental results of Ito *et al.* (Ref. 46). Note that, to within an additive constant, this scattering rate is the same as that found in our perturbation theoretic calculations. The arrow marks the crossover at T_*, discussed in the text.

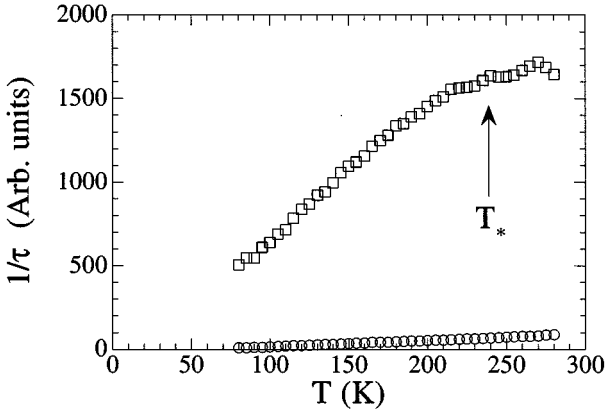

FIG. 13. The hot (top) and cold (bottom) scattering rates for $YBa_2Cu_4O_8$ obtained from the experimental results of Bucher *et al.* (Ref. 37). There scattering rates resemble closely those found in $YBa_2Cu_3O_{6.68}$, as might be expected from the similarities in their magnetic behavior. The arrow marks the crossover at T_*.

NMR experiments, because both T_{cr} and T_* are close to T_c for $YBa_2Cu_3O_7$, this result provides a further indication of the presence of the PG phase even in optimally doped 123 materials.

A similar analysis can be performed in single-CuO-layer materials: Two panels of Fig. 15 show the scattering rates at doping levels $x=0.10$, $x=0.15$ in 214 compound. Much like $YBa_2Cu_3O_{6.68}$, one observes the saturation of the scattering rate in the hot region and it is only for a particular anisotropy level that the resistivity in the optimally doped 214 material is approximately linear in T below T_*^r. In fact, as pointed out in Ref. 36, a crossover in resistivity exists even in this material, but is so minor that one usually assumes that $\rho_{xx} \propto T$ at all temperatures. As mentioned before, in the 214 family T_*^r is considerably larger than T_*.

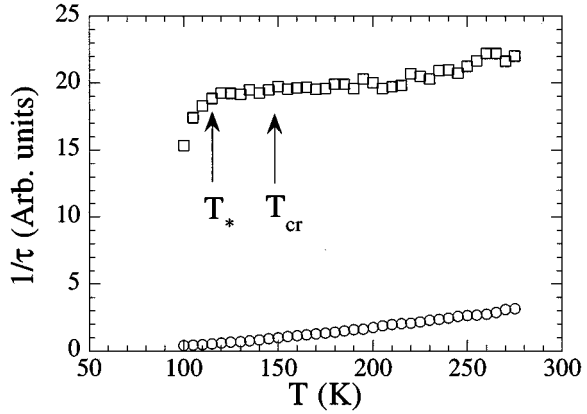

FIG. 14. The hot (top) and cold (bottom) scattering rates for $YBa_2Cu_3O_7$ obtained from the experimental results of Rice *et al.* (Ref. 45). Note that $1/\tau_{hot}$ shows a crossover from the $\Delta k=0$ result in Fig. 3 to the same result in Fig. 2, which should occur near T_{cr}, marked in the figure by an arrow. $1/\tau_{hot}$ weakly increases with temperature for $T \ll T_{cr}$ (see Fig. 2). T_* is the crossover temperature equivalent to those shown in Figs. 11 and 13. Note that $1/\tau_{cold}$ is approximately quadratic in temperature, in agreement with our perturbation theory calculations.

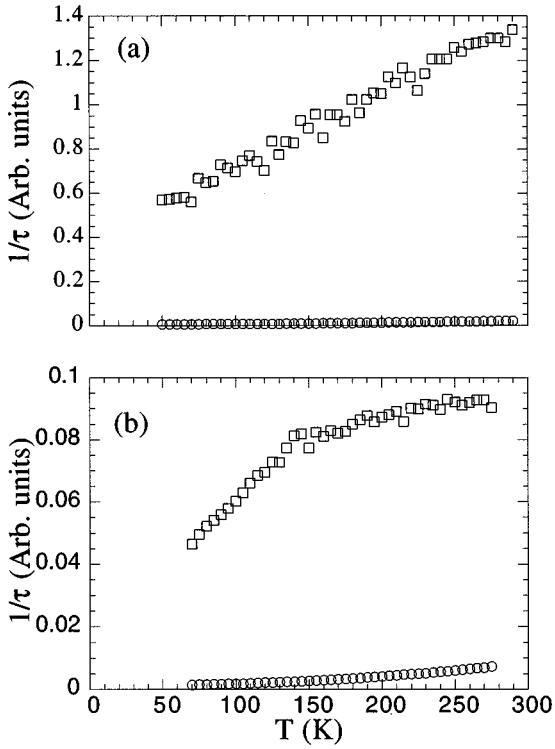

FIG. 15. The hot (top) and cold (bottom) scattering rates for two 214 compounds obtained from the experimental results of Hwang *et al.* (Ref. 36). The top (bottom) panel shows the results for $x=0.10$ ($x=0.15$) doping level. In the bottom panel the crossover temperature T_* is clearly observed in $1/\tau_{hot}$, as expected in the NAFL model.

Finally we consider the overdoped single-layer materials: Figure 16 shows the scattering rates for the overdoped 15-K Tl 2201 compound. First, one immediately notices that the anisotropy of scattering is not nearly as pronounced as in previous graphs. Note that in this case R_∞ is very well known and thus one can consider this reduced anisotropy in scattering rates quantitatively as well. We remark that both scatter-

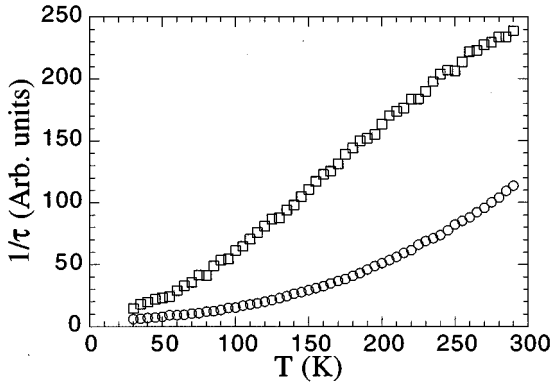

FIG. 16. The hot (top) and cold (bottom) scattering rates for a 15-K 2201 Tl compound obtained from the experimental results of Mackenzie *et al.* (Ref. 44). Note that the anisotropy of scattering is considerably reduced in overdoped materials, due to the smaller correlation length and the strong fermionic damping, manifested in a larger value of ω_{sf} (see text).

ing rates have nearly as strong T dependence as in the previous cases, over the entire T range. Moreover, the scattering rates shown here again closely resemble the calculated result for larger Δk in Fig. 2.

V. NUMERICAL RESULTS

In the previous sections we have established the relationship between the crossovers in the magnetic spectrum of cuprates and their transport properties analytically. However, it is unclear whether such an analysis, based on back-of-the-envelope calculations, can account for the experimental results quantitatively. In this section we present our numerical results for the transport coefficients in NAFL's: We show that for spin-fluctuation and band parameters chosen from NMR, INS, and ARPES measurements, the NAFL model indeed reproduces experimentally obtained results. We compare our results to experiments performed on several compounds of interest, examine the sensitivity of our results to the input parameters of the theory, and address several important questions regarding realistic materials, including the strong a-b plane anisotropy observed in a number of bilayer compounds.

The method used to obtain the results presented here has already been discussed elsewhere[31] and hence we only review it briefly. We study the transport in NAFL's by solving the Boltzmann equation (BE) numerically. We obtain the displacement of the quasiparticle (fermionic) distribution function

$$f_0(k)-f(k)=\Phi_k\left(\frac{\partial f_0(k)}{\partial \epsilon}\right) \tag{47}$$

as a function of momentum k, temperature, and frequency on a fine mesh of points in the Brillouin zone, using a standard relaxation method. The transport coefficients are then obtained from

$$\mathbf{j}=e\sum_k \Phi_k \mathbf{v}_k\left(\frac{\partial f_0}{\partial \epsilon}\right), \tag{48}$$

where $\mathbf{v}=\nabla \epsilon_k$. We assume that the interaction present in the collision integral in the BE is given by Eq. (1). The numerical method can be described as follows: We start from a reasonable choice of Φ_k, which we then use to calculate the collision integral, which in turn provides for a new value of Φ_k. The iteration procedure is stopped when the difference between two subsequent values of Φ_k is smaller than a given tolerance.

In our earlier numerical work,[23,31] we demonstrated the viability of a NAFL description of transport in the cuprates. By using spin-fluctuation spectra seen in NMR experiments, we were able to obtain both qualitative and quantitative agreement with the analysis presented in Sec. III and Sec. IV. However, for the band parameters, doping level, and spin-fluctuation spectrum we assumed that, for optimally doped $YBa_2Cu_3O_7$, the crossover temperature T_0 was high compared to that seen experimentally, while ρ_{xx} exhibited FL behavior up to temperatures ~ 200 K. Because T_0 was large, on extrapolating our linear-in-T results for ρ_{xx} to zero temperature, we found a large negative intercept. Moreover, although the calculated Hall coefficient decreased with increasing temperature, it displayed a far weaker temperature dependence than that seen experimentally. Our results thus resembled those found for overdoped cuprates, rather than an optimally doped sample.

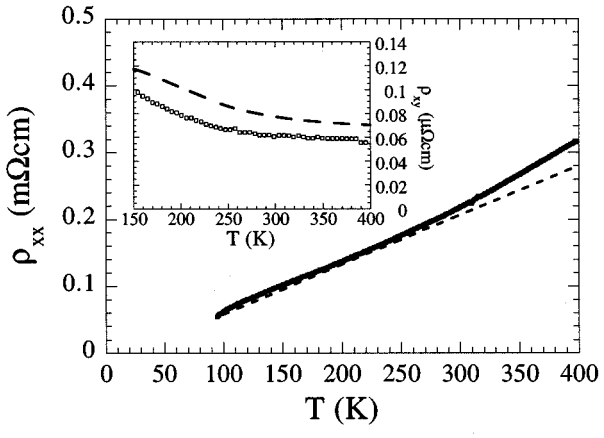

FIG. 17. A comparison of our calculated result for $\rho_{xx}(T)$ with the experimental result of Carrington *et al.* (Ref. 20). The coupling constant $g\approx 0.48$ eV has been adjusted to yield the best fit. Note that in this case T_0, Eq. (32), is of order 20 K and hence one observes a very small negative intercept of the resistivity, ~ 20 $\mu\Omega$ cm, as seen in experiment. Inset: the Hall resistivity as a function of temperature in comparison with experiment for the same system.

On the basis of the analysis presented in Sec. III, we can identify several potential causes for these discrepancies. First, the actual value of $\omega_0 \equiv \omega_{SF}\xi^2$ in optimally doped 123 is $\lesssim 60$ meV,[32] rather than the larger value, $\omega_0=76$ meV, adopted in these calculations. Second, the spin fluctuation spectrum was assumed to possess a commensurate peak, rather than the four incommensurate peaks which a recent analysis of NMR and INS results suggests might provide a better fit to experiments on the system.[32] Third, the doping level was taken to be $n\sim 0.25\%$, while the local density approximation (LDA) calculations of bonding and antibonding in bilayer materials discussed below suggest a considerably lower doping level might be more appropriate. Each of these effects acts to bring about either a lower value of T_0, an increase in the linear-in-T regime of ρ_{xx}, and/or an increased temperature dependence of R_H. To explore their combined influence, we carry out a numerical solution of the BE for a representative ''standard'' 123 material for which $n=20\%$, $\omega_0=60$ meV, and $\omega_{SF}(\mathrm{K})=60+0.6T$ (K); the band spectrum was assumed to be $t=0.2$ eV, $t'=-0.35t$, which is slightly different from the unrenormalized LDA spectrum,[40] while the incommensurate peaks in the spin spectrum are assumed to lie along the diagonals, at $\mathbf{Q}_i=\mathbf{Q}+(\pm 0.1\pi,\pm 0.1\pi)$, as proposed by Zha *et al.*[32]

In Fig. 17 we compare our calculated resistivity as a function of temperature with the experimental results obtained for optimally doped $YBa_2Cu_3O_7$. The coupling constant g, which sets the scale for the magnitude of the resistivity, has been adjusted to $g=0.48$ eV, in order to obtain the best fit. Clearly, the calculated result agrees very well with the data down to temperatures only slightly above T_c. Note that the extrapolated value of ρ_{xx} at $T=0$ is now quite small, as is seen in the experiment. On the other hand, the Hall coeffi-

cient, shown in the inset of the figure, is strongly temperature dependent, with a relative decrease which is approximately the same as that seen experimentally in the temperature interval 150–400 K, although the exact shape of R_H is not the same. However, as mentioned above, a better knowledge of the band structure, including the chain contribution, and of the effective interaction $V_{\rm eff}$ for $\mathbf{q}$ away from $\mathbf{Q}_i$ might well remove this problem. Moreover, a quick look at Eq. (45), as well as Eqs. (31) and (34), indicates that the FS reduction (i.e., decreasing $\Delta k_{\rm max}$), with the approaching PG phase at low temperatures, should provide for an additional temperature dependence of R_H. Our calculated R_H saturates at higher T, to a somewhat higher value than that seen experimentally, implying that a different value of the doping level should be used; nevertheless, our choice of parameters would seem quite reasonable [see Eq. (41)]. Another reason for a discrepancy in the shape of R_H lies in the fact that we have calculated this quantity assuming a tetragonal lattice, rather than the orthorhombic one found in $YBa_2Cu_3O_7$. Recent measurements[41] on twinned and detwinned crystals of this material show a considerable difference in R_H, indicating the importance of including the *a*-*b* plane anisotropy in the calculation. We return to this point at the end of this section.

The doping level used in this calculation is somewhat low. If one assumes that every oxygen atom doped into the 123 system extracts a single hole from CuO planes, the doping level of the optimally doped $123O_{6.93}$ should be somewhat higher, $n\approx 23\%$. On the other hand, simple arguments, based on LDA calculations, suggest that in bilayer materials, such as 123 compounds, there are two bands, bonding and antibonding, separated by twice the hopping matrix element between the CuO layers, $t_\perp$ (see Refs. 40 and 42). If one assumes that $t_\perp$ is weakly momentum dependent, one finds that the top (antibonding) band is more heavily doped, while the bottom (bonding) band should be close to half filling, regardless of the oxygen content.[42] Since the interaction between quasiparticles is much weaker in the metallic state of cuprates than it is in the insulating state, the nearly half-filled bonding band has a larger value of v_f and should provide the dominant contribution to the conductivity in the bilayers [see Eq. (31)]. Hence the doping level chosen here, $n=20\%$, may be quite reasonable for 123 and 124 compounds.

To study the effect of doping on the resistivity at fixed spin fluctuation spectra we have calculated $\rho_{xx}(T)$ for the same values of the spin and band parameters as in our ''standard model,'' but with the chemical potential adjusted to yield an $n=30\%$ doping level, and compared it to the above case in Fig. 18. Clearly, ρ_{xx} ceases to be linear in T at lower temperatures, while continuing to exhibit typical FL behavior as $T\rightarrow 0$. In the same figure we also show the influence of incommensuration, by plotting $\rho_{xx}(T)$ for the same representative set of parameters as above, but with a commensurate spin-fluctuation spectrum. Although the commensurate result has a slope at higher temperatures which is remarkably similar to the incommensurate (representative) one (due to the fact that ρ_{xx} is independent of ω_0 above T_0 [see Eq. (31)]), we again observe FL-like behavior at lower temperatures. In both cases the explanation is simple: Enlarging $\Delta k_{\rm max}$ leads to an increase in T_0; this can be achieved either by increasing the doping level, which increases the size of the FS, or by removing the extra hot spots brought about by incommensuration. Figure 18 demonstrates quite clearly that the behavior of the resistivity is sensitive to the choice of band parameters and leads us to conclude that self-consistent calculations which take into account changes in the quasiparticle interaction should be used in comparing with experiment.[30] On the other hand, assuming that the magnetic (band) parameters are well known, our model can be used to put constraints on the allowed band (magnetic) parameter values.

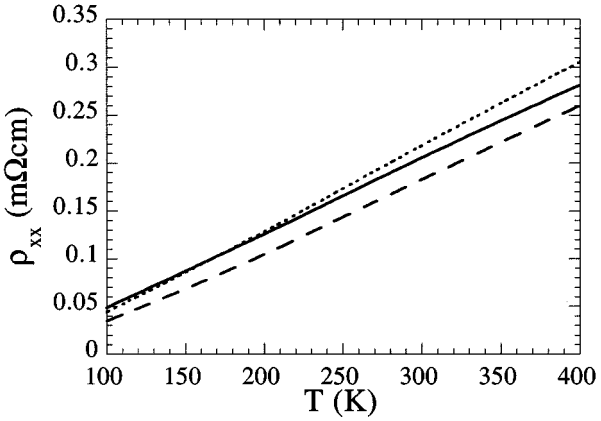

FIG. 18. The sensitivity of $\rho_{xx}(T)$ with respect to the band and incommensuration parameters. The solid line shows the same $\rho_{xx}(T)$ as in Fig. 17 with $g=1$ eV. The dashed and dotted lines show $\rho_{xx}(T)$ at a $n=30\%$ doping level and zero incommensuration ($\Delta Q=0$), respectively.

Next we examine the dependence of ρ_{xx} and σ_{xy} on $\omega_{\rm sf}=A+BT$. In Fig. 19 we plot the resistivity as a function of temperature for four different values of A and B: We show the cases where $A=20$ K and $B=0.2$, the case where $A=0.6$ and B is the same, the case where B is 0.6 and A is the same, and the case where $\omega_{\rm sf}=60+0.6T$. The band parameters are set to $t=250$ meV, $t'=-0.45t$, and the doping level is $n=15\%$; the coupling constant is set to $g=1$ eV. In agreement with our analysis in Sec. III, a large value of A,

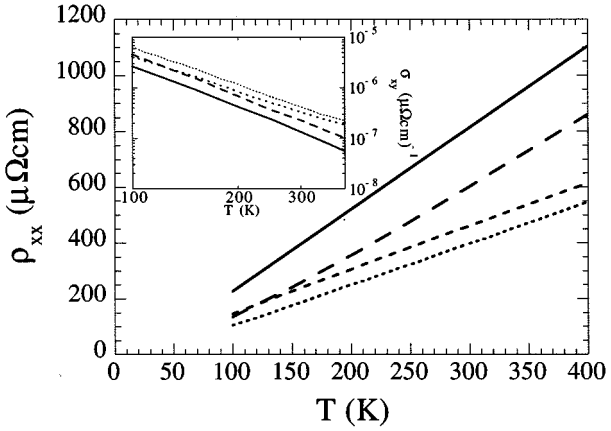

FIG. 19. The sensitivity of $\rho_{xx}(T)$ with respect to the changes in spin-fluctuation parameters. The curves correspond to (top to bottom) $\omega_{\rm sf}=20+0.2T$ (K), $60+0.2T$ (K), $20+0.6T$ (K), and $60+0.6T$ (K), respectively. All other parameters are assumed the same as in Fig. 18. Inset: $\sigma_{xy}(T)$ for the input parameters defined in the figure.

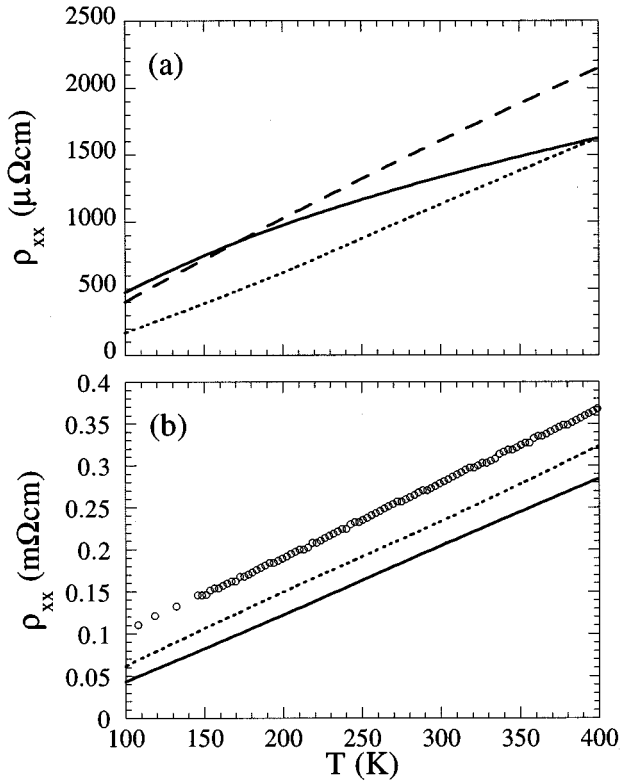

FIG. 20. (a) $\rho_{xx}(T)$ in the PG regime: the parameters used are $\xi^{-1}=0.1+T/1000$ (K), $\omega_{sf}\xi=50$ meV, $g=1$ eV, and $n=15\%$. The solid, dashed, and dotted lines correspond to $-t'/t=0.2$, 0.3, and 0.4, respectively. The effective interaction is assumed to have incommensurate peaks at $\mathbf{Q}+(\pm\Delta Q,0)$ and $\mathbf{Q}+(0,\pm\Delta Q)$, where $\Delta Q=0.25\pi$. The three curves show a vast difference in the crossover temperature $T_0(T)$. (b) $\rho_{xx}(T)$ in comparison with experiment (Ref. 36). The solid line corresponds to $t'=-0.3t$, with g adjusted to yield the same slope as seen experimentally. The dashed line corresponds to $t'=-0.25t$, with the FL scattering included (see text).

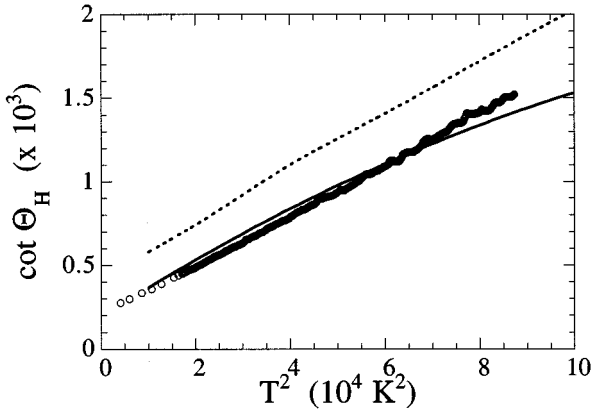

FIG. 21. Comparison of the calculated value of $\cot\Theta_H$ with experiment (Ref. 36). The solid (dashed) line corresponds to the result depicted by the solid (dashed) line in Fig. 20(b).

corresponding to an enhanced damping of spin fluctuations due to spin-fermion interactions, shifts the resistivity down; it leads to a higher value of T_0 in Eq. (31) and only marginally anomalous scattering rates even in hot regions of the FS, in agreement with the result presented in Fig. 16.

On the contrary, increasing the value of B only changes the slope of the resistivity curves shown in Fig. 19, but does not much affect the behavior with respect to the origin. This is to be expected, since according to Eq. (19) the term BT in ω_{sf} acts in conjunction with the πT term in $\sqrt{\pi T+\omega_{sf}[1+(\Delta k)^2\xi^2]}$ to bring about linear-in-T resistivity. However, since in all experimentally studied samples $B\ll\pi$, the effective value of $T_0\sim\omega_0(\Delta k_{max})^2/2(\pi+B)$ differs only slightly from that quoted in Eq. (32). As noted in Sec. III, for practically all cuprates BT is never large enough to produce the $T^{1/2}$ behavior of the resistivity discussed there, which is found at $T\sim\omega_0(\Delta k_{max})^2$, provided the FS is large enough. Hence, the crossover at T_*^r, where a curvature resembling $T^{1/2}$ is found in many underdoped samples at $T\geq T_*$, has to be attributed to a small value of Δk_{max} resulting from the FS evolution. Finally we note that the Hall conductivities for all of the above cases obey a T^{-3} law quite well, as shown in the inset of the figure, although due to the large value of T_0 the Hall resistivity may be only weakly temperature dependent.

We turn now to the $z=1$ PS regime. As indicated in Sec. III, the resistivity is linear in T for $T>T_0$ regardless of whether or not T_0 is temperature dependent. However, since $\xi\sim 1/T$ in this regime, the condition $\xi\Delta k<1$ is satisfied over most of the FS at relatively low temperatures. In this case the resistivity due to spin-fluctuation scattering tends to a constant, since $T\gg 2\pi T_0$. To further explore the PS regime, we solve the BE numerically for a representative member of the 2-1-4 system ($\hat{c}=\omega_{sf}\xi=50$ meV, $\xi^{-1}=0.1+T/1000$ K, $g=1$ eV, $n=15\%$, $t=250$ meV) and several values of t' ($-t'/t=0.2$, 0.3, and 0.4, respectively). Our results are shown in Fig. 20(a). In all of the cases displayed there we have assumed that the effective interaction has incommensurate peaks at $\mathbf{Q}_i=\mathbf{Q}+(\pm\Delta Q,0)$ and $\mathbf{Q}+(0,\pm\Delta Q)$, with $\Delta Q=0.25\pi$, in order to be consistent with neutron scattering experiments performed in 214 materials at sufficiently high doping levels.[32] For $t'=-0.4t$ the FS is relatively large, as is the corresponding $T_0(T)$. As a result one observes a crossover to linear-in-T resistivity at $T\sim 200$ K from the low-T Fermi-liquid-like behavior. For $t'=-0.2t$ the FS is always close to the Brillouin zone boundary and hence the effective Δk_{max} is small, $\Delta k_{max}\sim 0.1$. Hence the condition $T=2\pi T_0(T)$ is satisfied for $T\sim 1000$ K, and the resistivity deviates from linearity already at $T=150$. Obviously, in the intermediate case $\rho_{xx}\propto T$ over an extended temperature range. We conclude that the resistivity is very sensitive to changes in band parameters, especially when T_0 is a strong function of temperature.

The parameters used in Fig. 20(a) are close to those found for $La_{1.85}Sr_{0.15}CuO_4$ material in the PS regime.[28,32] In Fig. 20(b) we compare $\rho_{xx}(T)$, obtained for $t'=-0.33t$ (solid line), to experiment. The coupling constant has been adjusted to yield the same slope as the experimental curve. Obviously even in this case the calculated resistivity exhibits the features shown in Fig. 20(a), but the fit is quite good, especially keeping in mind the fact that the experimental result is subject to disorder. On the other hand, when one compares $\cot\Theta_H$ in these two cases (solid line in Fig. 21), the fit, although remaining reasonable, is not as good. The curvature

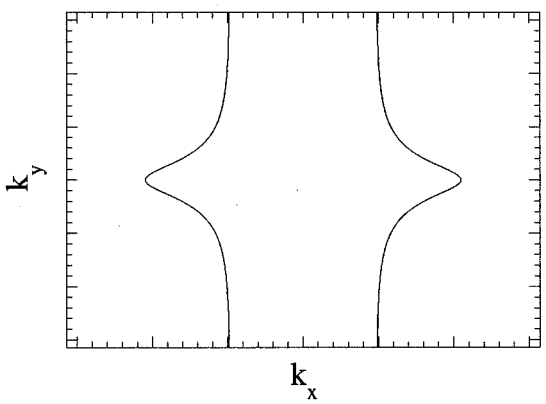

FIG. 22. A model FS for a system with strong a-b plane anisotropy. The anisotropy parameter is assumed to be $a=0.5$ [see Eq. (49)], and the doping level is $n\approx 15\%$.

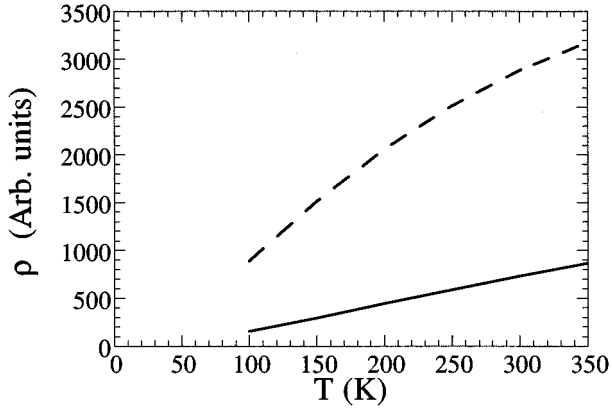

FIG. 23. The resistivities along a and b crystallographic directions as a function of temperature for the system with the FS depicted in Fig. 22, using the spin-fluctuation parameters appropriate to $YBa_2Cu_4O_8$ system. Note that there is not only a large quantitative difference, but a qualitative difference as well, as is seen in experiment. The anisotropy of the distribution of the hot regions leads to the anisotropy of the resistivities.

of the calculated result (and lack thereof in the experimental result) implies that the cold regions of the FS are too small in the calculation, whence $\cot\Theta_H \sim T^{1.6}$, rather than the T^2, behavior frequently seen, although some samples of this material have the smaller exponent in $\cot\Theta_H$ found here. However, even for a small value of t', the addition of a Fermi liquid term $\chi_{\rm FL}=\chi_0(T)/[1-i\pi\omega/\Gamma(T)]$, to the effective interaction, makes the resistivity appear linear in T up to higher temperatures and the agreement with experiment for the Hall effect much better, as shown by the dashed line in Figs. 20 and 21. In both cases we have used $\Gamma(T)=(0.5-T/2500)$ eV and $\chi_0(T)=1+0.4T/100$ states/eV, the values obtained from the fits to NMR measurements.[43] This is as expected, since adding a Fermi liquid term affects predominantly the cold regions of the FS and its effect is similar to that of the strong band renormalization present in the PS regime.

We next consider the issue of the a-b plane anisotropy. Although found in practically all cuprates, this anisotropy is especially pronounced in materials with CuO chains, leading to quite different transport results along different crystallographic directions. In principle, these are two reasons for an anisotropic resistivity: The chains can form a conducting band, or the chain bands hybridize with oxygen bands in CuO plane, producing an anisotropic quasiparticle effective mass. Since the chains in, e.g., $YBa_2Cu_3O_7$ are very close to the CuO planes and the oxygen p orbitals are rather large, we believe that the latter effect must dominate. In order to simulate its effect on the in-plane resistivity we consider a 2D band with anisotropic hopping integrals: We alter the first term in Eq. (2) to read

$$-2t(\cos k_x + a\cos k_y). \tag{49}$$

In Eq. (49) the anisotropy parameter a lies between 0 and 1; obviously, $a=1$ in tetragonal systems. A FS for an anisotropic system with $a=0.55$ and the doping level $n=10\%$ is shown in Fig. 22. Although this shape of the FS is somewhat incompatible with that observed in, e.g., the 124 material, one must keep in mind that strictly speaking a single-band model, such as that considered here, is an oversimplification; we only use the present model in order to qualitatively explain the physics in the above material.

In Fig. 23 we show the resistivities for the current running along x and y directions for the band depicted by the FS in Fig. 22. We assume that $\omega_{\rm sf}(K)=20+0.2T$, which is close to $\omega_{\rm sf}$ found in 124 materials. However, we retain the $z=2$ scaling regime in order to make the comparison with previous results easier. Clearly, not only are the magnitudes of the two resistivities different, but their temperature dependence is also different; indeed our results for ρ_{xx} and ρ_{yy} resemble those found in the 124 material. The lower curve $[\rho_{xx}(T)]$ appears to have a considerable negative intercept, indicating a large value of T_0, as in overdoped materials. The upper curve $\rho_{yy}(T)$ exhibits a crossover at $T\sim 300$ K, similar to that observed experimentally at T_*^r in underdoped cuprates. This quite different behavior arises from the modified positions of the hot spots: As may be seen on examining the FS shown in Fig. 22, the hot spots are now located at points $(1,\pm\pi)$ and $(\pi-1,0)$ and symmetry-related points on the FS; i.e., they are asymmetric with respect to the inversion of the x and y axes and cannot be obtained by drawing the usual magnetic Brillouin zone boundary. For current running along the x direction, a large segment of the FS, roughly along the $(1,y)$ direction, can be displaced in transport (the vertex function v_x is large at these k vectors) and, more importantly, these segments of the FS are far from the hot spot at $(1,\pm\pi)$, so that it is necessary to balance the hot and cold regions, to arrive at a ρ_{xx} which is linear in T. For current running along the y direction, the vertex v_y is small almost everywhere on the FS [see Eq. (48)] and the hot spots sit in the middle of the region of the FS where v_y is the largest, further reducing the conductivity in this case. Effectively the FS appears to be small, producing the anomalous (nonlinear with negative curvature) $\rho_{yy}(T)$ seen in the figure. Note that the Hall conductivity is proportional to T^{-3}, as seen in Fig. 24. We also note that our result for σ_{xy} is the

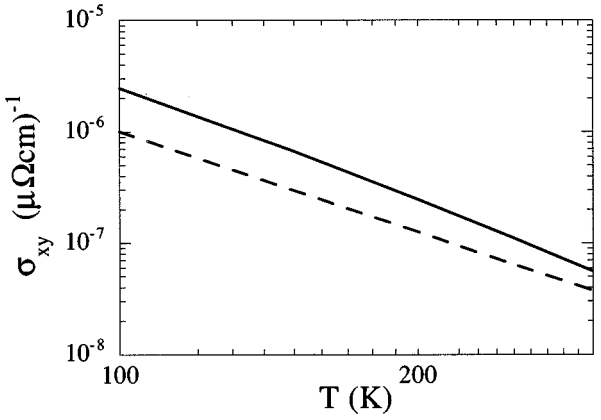

FIG. 24. The Hall conductivity as a function of temperature for the system depicted in Fig. 23. Note that, as usual, σ_{xy} reflects an average contribution of the hot and cold regions and hence is proportional to T^{-3} as in the isotropic case (see Fig. 17 and its inset).

same to within a few percent for both current directions, which serves as a nice check of the quality of numerics in this case.

We make another important comment regarding this result: Unlike the case of 124 material, where T_*^r is very close to T_*, so that the anomalous behavior of the resistivity occurs at least in the pseudoscaling ($z=1$) regime if not in the pseudogap one, here we have similar behavior with $z=2$. We again conclude that the crossover at T_*^r is closely related to the effective size of the FS and is less closely related to a particular magnetic regime.[29] However, we must keep in mind that the FS here is reduced artificially (by introducing a very large anisotropy). In reality, magnetic fluctuations alter the shape of the FS as the system enters into the pseudogap regime. Moreover, one cannot obtain a similar anomalous behavior of ρ_{yy} using a large Fermi surface and the same spin-fluctuation parameters as those utilized here, and hence this result serves as a further indication that the pseudogap regime involves an evolution of the FS.

VI. CONCLUSIONS

We have performed an analysis of the in-plane longitudinal and Hall conductivities (resistivities), in terms of the NAFL model, using both perturbation theory and numerical methods. From our perturbation theory results we obtained an analytical expression for the scattering rate as a function of temperature for an arbitrary point on the FS, as well as empirical expressions for ρ_{xx} and ρ_{xy}. The results are then used to study analytically the crossovers in transport in various temperature regimes. Assuming a particular geometry of the FS, we obtained phenomenological expressions for both ρ_{xx} and ρ_{xy} which we used to analyze the experimental results and gain further insight into the scattering rates. Finally, we performed a set of numerical calculations, verifying for a realistic set of input parameters that the NAFL model yields results in agreement with experiment.

Our analytical results display a relatively strong anisotropy of scattering rates around the FS, leading to a complex morphology of both ρ_{xx} and ρ_{xy}, in contrast to the common belief that in all cuprates $\rho_{xx} \propto T$ and $\rho_{xy} \propto 1/T$ over the entire temperature regime. A close examination of the available experimental data shows that the *universality* of the temperature behavior of both ρ_{xx} and ρ_{xy} is quite marginal over larger temperature regions; i.e., only extremely clean, optimally doped samples of 123 show $\rho \sim \rho_0 + \alpha T$ with $\rho_0 \sim 0$ and $\cot\Theta_H \sim T^2$. In fact even these materials show small deviations from this behavior at low temperatures; e.g., optimally doped 214 compounds show a nonvanishing intercept of $\cot\Theta_H$ at $T=0$. All other doping levels show more or less pronounced deviations from the above *optimal* behavior at *low* temperatures, in agreement with the NAFL model. We therefore conclude that the *optimally* doped compounds are rather unique and the temperature variation of their transport coefficients, in particular their Hall effect, is somewhat accidental. The calculated results for the scattering rates are found to be in detailed qualitative agreement with those coming from the fits to the experimental data. It is remarkable how systematically the scattering rates vary with temperature and doping and how precisely they reflect the magnetic properties in cuprates.

Finally our numerical results show reasonable agreement with experiment for a realistic set of spin-fluctuation and band parameters in both the $z=1$ and $z=2$ scaling regimes. We find that improved quantitative agreement can be achieved through the inclusion of strong-coupling effects, which bring about a temperature-dependent quasiparticle band structure. In addition, we show that the NAFL model provides a natural explanation of the unusual temperature dependence of the resistivities along different directions in 124 material.

How meaningful is the agreement between our NAFL model calculation and experiment, given the large number of parameters ($\omega_{\rm sf}$, ξ, $\Delta k_{\rm max}$, and g) which enter the theory? We recall that $\omega_{\rm sf}$ and ξ are fixed by NMR and neutron scattering measurements, so that the additional parameters in the problem are the band parameters t, t', and μ, which determine the geometry of the Fermi surface at high temperatures, and the coupling constant g. We have shown that influence of the band parameters can be characterized by a single parameter $\Delta k_{\rm max}$, which is a measure of the effective size of the Fermi surface. For $YBa_2Cu_3O_{6+x}$ even this parameter can be estimated quite accurately from ARPES measurements, so that for this system the only free parameter is g. For $La_{2-x}Sr_xCuO_4$, we have chosen the band parameters which produce incommensurate peaks in the bare particle-hole bubble and lead to a magnetic susceptibility in agreement with neutron scattering data, but strictly speaking in the absence of ARPES data for this compound, $\Delta k_{\rm max}$ should be regarded as a second free parameter. We conclude that given the quite small number of free parameters in our theory, the agreement with experiment is indeed meaningful, and provides an unambiguous demonstration that the NAFL model is capable of explaining the anomalous transport properties measured in the cuprate superconductors, ranging from the linear-in-T resistivity found to extend down to 10-K in underdoped polycrystalline Bi-Sr-Ca-Cu-O samples (which become superconducting only at this temperature[47]) to the high temperature (up to $\sim$800 K) linear-in-T resistivity found in optimally doped $La_{2-x}Sr_xCuO_4$.

It is straightforward to extend the NAFL model to optical

frequencies and to take into account the influence of impurities and we will report on these results in future publications.

ACKNOWLEDGMENTS

We are indebted to P. W. Anderson, A. Chubukov, V. Barzykin, B. Batlogg, G. Blumberg, G. Boebinger, P. Coleman, J. Giapintzakis, D. Ginsberg, R. Hlubina, R. Laughlin, A. Leggett, M. Lercher, N. P. Ong, T. M. Rice, Q. Si, C. Slichter, A. Shegoliev, R. Stern, D. Strong, T. Timusk, S. Trugman, and J. Wheatley for stimulating conversations on these and related topics. We thank the National Center for Supercomputing Applications for a grant of computer time. This research is supported in part by NSF through Grant Nos. NSF-DMR 89-20538 (MRL at UIUC) and NSF-DMR 91-20000 (STCS).

[1] Recent reviews of the NAFL approach may be found in D. Pines, Physica C **235-240**, 113 (1994); in *High Temperature Superconductivity and the C^{60} Family*, edited by H. C. Ren (Gordon and Breach, New York, 1995), pp. 1–32.

[2] See, e.g., C. P. Slichter, in *Strongly Correlated Electronic Systems*, edited by K. S. Bedell *et al.* (Addison-Wesley, New York, 1994).

[3] T. R. Chien, Z. Z. Wang, and N. P. Ong, Phys. Rev. Lett. **67**, 2088 (1991).

[4] See, e.g., Y. Iye, in *Physical Properties of High Temperature Superconductors*, edited by by D. M. Ginsberg (World Scientific, Singapore, 1992), Vol. 3.

[5] P. W. Anderson, Science **235**, 1196 (1987).

[6] S. Chakravarty and P. W. Anderson, Phys. Rev. Lett. **72**, P3859 (1994).

[7] P. A. Lee and N. Nagaosa, Phys. Rev. B **46**, 5621 (1992); N. Nagaosa and P. A. Lee, *ibid.* **45**, 966 (1992).

[8] B. L. Altshuler, L. B. Ioffe, and A. J. Millis, Phys. Rev. B **52**, 415 (1995).

[9] See, e.g., C. M. Varma, P. B. Littlewood, S. Schmitt-Rink, E. Abrahams, and A. E. Ruckenstein, Phys. Rev. Lett. **63**, 1996 (1989).

[10] P. W. Anderson, Phys. Rev. Lett. **67**, 2092 (1991).

[11] C. M. Hurd, in *The Hall Effect and Its Applications*, edited by C. I. Chien and C. R. Westgate (Plenum, New York, 1980).

[12] P. W. Anderson (private communication).

[13] P. Coleman, A. J. Schofield, and A. M. Tsvelik, Phys. Rev. Lett. **76**, 1324 (1996).

[14] S. G. Kaplan, S. Wu, H.-T. S. Lihn, H. D. Drew, Q. Li, D. B. Fenner, Julia M. Phillips, and S. Y. Hou, Phys. Rev. Lett. **76**, 696 (1996).

[15] A. S. Alexandrov, A. M. Bratkovsky, and N. F. Mott, Phys. Rev. Lett. **72**, 1734 (1994).

[16] A. T. Fiory and G. S. Grader, Phys. Rev. B **38**, 9198 (1988).

[17] Y. Ando, G. S. Boebinger, and A. Passner, Phys. Rev. Lett. **77**, 2065 (1996).

[18] G. Levin and K. F. Quader, Phys. Rev. B **46**, 5872 (1992).

[19] D. M. Newns *et al.*, Phys. Rev. B **43**, 3075 (1991).

[20] A. Carrington, A. P. Mackenzie, C. T. Lin, and J. R. Cooper, Phys. Rev. Lett. **69**, 2855 (1992).

[21] R. Hlubina and T. M. Rice, Phys. Rev. B **51**, 9253 (1995); **52**, 13 043 (1995).

[22] M. Lercher and J. M. Wheatley, Phys. Rev. B **52**, R7038 (1995).

[23] B. P. Stojković and D. Pines, Phys. Rev. Lett. **70**, 811 (1996).

[24] S. Trugman, Phys. Rev. Lett. **65**, 500 (1990); Phys. Rev. B **37**, 1597 (1988).

[25] J. H. Kim, K. Levin, and A. Auerbach, Phys. Rev. B **39**, 11 633 (1989).

[26] E. Dagotto, A. Nazarenko, and M. Boninsegni, Phys. Rev. Lett. **73**, 728 (1994).

[27] N. Bulut, D. J. Scalapino, and S. R. White, Phys. Rev. B **50**, 7215 (1994).

[28] V. Barzykin and D. Pines, Phys. Rev. B **52**, 13 585 (1995).

[29] A. V. Chubukov, D. Pines, and B. P. Stojković, J. Phys. Condens. Matter **8**, 10 017 (1996).

[30] P. Monthoux and D. Pines, Phys. Rev. B **47**, 6069 (1993); **49**, 4261 (1994) and references therein.

[31] B. P. Stojković, Philos. Mag. B **74**, 529 (1996).

[32] Y. Zha, V. Barzykin, and D. Pines, Phys. Rev. B **54**, 7561 (1996).

[33] J. H. Ziman, *Electrons and Phonons* (Oxford University Press, Oxford, 1960).

[34] G. Rickayzen, *Green's Functions and Condensed Matter Physics* (Academic Press, London, 1980).

[35] A. V. Chubukov, D. K. Morr, and K. A. Shakhnovich, Philos. Mag. B **74**, 563 (1996).

[36] For experimental results in 214 compounds see, e.g., H. Takagi *et al.*, Phys. Rev. Lett. **69**, 2975 (1992); H. Y. Hwang *et al.*, *ibid.* **72**, 2636 (1994).

[37] B. Bucher *et al.*, Phys. Rev. Lett. **70**, 2012 (1993).

[38] See, e.g., N. P. Ong, in *Physical Properties of High Temperature Superconductors*, edited by D. M. Ginsberg (World Scientific, Singapore, 1990), Vol. 2.

[39] J. M. Harris, Y. F. Yan, and N. P. Ong, Phys. Rev. B **46**, 14 293 (1992).

[40] O. K. Anderson *et al.*, Phys. Rev. B **49**, 4145 (1994).

[41] A. Shegolyev and J. Giapintzakis (private communication).

[42] G. Blumberg, B. P. Stojković, and M. V. Klein, Phys. Rev. B **52**, 15 741 (1996).

[43] H. Monien, P. Monthoux, and D. Pines, Phys. Rev. B **43**, 275 (1991).

[44] A. P. Mackenzie, S. R. Julian, D. C. Sinclair, and C. T. Lin, Phys. Rev. B **53**, 5848 (1996).

[45] J. P. Rice, J. Giapintzakis, D. M. Ginsberg, and J. M. Mochel, Phys. Rev. B **44**, 10 158 (1991).

[46] T. Ito, K. Takenaka, and S. Uchida, Phys. Rev. Lett. **70**, 3995 (1993).

[47] S. Martin *et al.*, Phys. Rev. B **41**, 846 (1990).